NRL Report 7477

Nuclear and Ion Beam Techniques for Surface and Near-Surface Analysis

ELIGIUS A. WOLICKI

Nuclear Sciences Division

December 13, 1972

NAVAL RESEARCH LABORATORY
Washington, D.C.

CONTENTS

PREFACE

The contents of this report have been submitted for publication in *Determination of Gases in Metals*, edited by Melnick, Lewis, and Holt, to be published by John Wiley and Sons, Inc. Printed with the permission of the publisher.

ABSTRACT

A survey is made of recent developments in the applications of ion beam techniques to surface analyses. Ion beams are taken to be charged atomic species such as protons, deuterons, helium-3, alpha particles, and others and the energies of interest, usually, but not always, are in the range from one million electron volts (MeV) upward. The discussion covers not only those techniques which are presently ready for application but also those which are still being investigated and developed in the laboratory. The objective of the discussion is to give the reader an overview of the present state of the art and, hopefully, sufficient information so that he can assess, for his own problems, whether a given technique may have advantages over more standard techniques.

Techniques are categorized according to whether they are based on charged particle activation analysis or on prompt radiation analysis. The discussion emphasizes prompt radiation analysis since this area is in general newer and less well known than is charged particle activation analysis. Subcategories discussed under prompt radiation analysis include: (a) high-energy backscattering, (b) channeling, (c) high-energy forward scattering, (d) low-energy backscattering, (e) heavy-ion-induced x rays, (f) nuclear reactions, and (g) nuclear resonance reactions. Numerous examples of actual analyses are discussed for each category. A comprehensive list of references, totaling 108 in number, is given.

NUCLEAR AND ION BEAM TECHNIQUES FOR SURFACE AND NEAR-SURFACE ANALYSIS

I. INTRODUCTION

In the past few years the field of surface analysis has seen the development of a surprising number of promising new physical methods based on the use of high-energy ion beams. Improvements and advances continue to be reported at a rapid pace at the time of this writing, and the field can well be said to be scientifically most interesting and exciting. In addition to the extensive literature which is developing in this area, the reader may find Refs. 1 through 7 useful in that they emphasize areas of current research interest.

Ion beams will be taken here to be charged atomic species such as protons, deuterons, helium-3, alpha particles, and others, and the energies of interest, usually but not always, will be in the range from one million electron volts (MeV) upward. These particles are, for the most part, useful only for surface analyses for the reason that their penetration ranges in solid matter are extremely short. At an energy of 2.0 MeV, for example, proton ranges in metals are typically about 50 μm and alpha particle ranges are about 6 μm.

The very powerful and important photon and electron beam techniques for studying surfaces such as Auger electron spectroscopy, low-energy electron diffraction (LEED), and electron spectroscopy chemical analysis (ESCA) will not be discussed since they are outside the author's purview. Use of these techniques is widespread and growing, and commercial equipment is available. Similar statements apply to the somewhat more recently developed technique of ion beam mass spectrometry. In this technique a heavy ion beam with approximately 10 keV energy is used to sputter away the sample surface, the sputtered ions being mass analyzed to provide not only a chemical analysis of the surface but also a depth profile for a selected element. Again the use of this technique is growing rapidly and the requisite equipment is available commercially.

While a few of the new techniques are close to routine application and others are clearly advancing in that direction, there are a number which are still being investigated and developed in the laboratory. In order that the text may remain germane to this changing area for a longer period than would otherwise be the case and at the same time be useful to the reader for anticipating future trends, the discussion will cover not only those techniques which are presently ready for application but others as well. The objective of the discussion will be to give the reader an overview of the present state of the art and, hopefully, sufficient information so that he can assess, for his own problems, whether a given technique may have advantages over more standard techniques.

Analysis for constituent chemical elements with ion beams from an accelerator consists of irradiating the sample with the ion beam and detecting the resulting

characteristic radiations. The irradiations are usually performed in vacuum, and the ion beam is generally magnetically analyzed so that it consists of a single atomic species and has a well-defined energy. Emitted radiations may be detected with Geiger-Mueller counters, proportional counters, scintillation, or solid-state detectors, the pulses from the latter three detectors being analyzed typically with a multichannel pulse-height analyzer. The reactions which occur between the incident ions and the atoms of the sample (target) depend on the energy of the ions and the atomic species of both the beam and the sample. An incident ion beam, a sample, and some of the typical emitted radiations are shown schematically in Fig. 1.

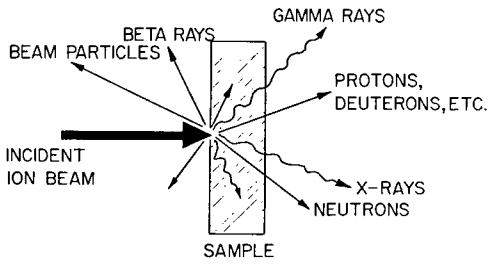

Fig. 1 — The interaction of an ion beam with a target sample and the various radiations which can be produced

The type of radiation and spectrum of pulse heights produced will be characteristic of the reactions induced by the incident beam in the constituent target elements. If the energy of the incident ion is great enough to overcome the electrostatic potential energy of repulsion which builds up as the ion approaches a target atom nucleus, then a nuclear reaction can occur. In such a case the emitted radiation will be nuclear in origin and will typically be a gamma ray, a charged nuclear particle which can be the same as or different from the incident ion, a neutron, or a beta particle. Because nuclear reaction characteristics can differ markedly between two isotopes of the same chemical element, the reaction products are specific not only to the element but to a particular isotope of that element. This property, which is commonly utilized in stable and radioisotope tracer work, makes possible some important applications also in materials analysis. Nuclear reactions have the disadvantage, however, that, with only a few exceptions which do not pertain to this discussion, they are not affected by chemical forces and so do not give information directly about the chemical compound form of the elements in a sample.

Radiations can be emitted from an irradiated sample also as a result of nonnuclear reactions. The two principal examples, for purposes of the present discussion, are heavy-ion-induced characteristic x rays and Rutherford or elastic scattering. The energies used for x-ray analysis with such beam particles as protons and alpha particles are most commonly in the MeV range. Rutherford scattering has been used for analysis with beam energies ranging from a few tenths of kiloelectron volts (keV) to MeV. Both of these techniques are of particular interest because they can often be used to analyze for many elements in the sample with a single irradiation.

The fact that many of the techniques discussed here require highly sophisticated and expensive equipment in the form of small nuclear accelerators, radiation detectors, and pulse-height analyzing systems has not been overlooked. Neither is there any intent to

underestimate the practical difficulties attendant to the wide use of these techniques because of the high equipment costs involved. The view is taken rather that there may be problems which cannot be satisfactorily solved in any other way which are sufficiently important so that technique costs will not be the dominant factor. In this connection it may be useful to call attention to the fact that there are a large number of nuclear accelerator facilities (8), primarily at universities but in industry also, and that many of these are currently interested in interdisciplinary problems in general and materials analysis problems in particular. It may be possible therefore, through one of these groups, to test the application of a given technique to a specific analysis problem when a need arises.

The relative advantages of nuclear and ion beam techniques, expressed for the cases where they can be applied, are that they can have excellent specificity, high sensitivity, and good accuracy. The latter characteristic, which is especially important in trace element work, results from the fact that, often, little or no sample processing is involved and the chances for introducing extraneous elements are thereby reduced. For metals in particular but for many other materials as well, the irradiations are in addition nondestructive so that elemental analysis on a particular sample does not preclude any other subsequent tests or measurements which may be desired.

The principal disadvantages are the high cost involved, as has previously been mentioned, and a low precision as compared to most standard analytical techniques. The disadvantage of high cost requires qualification. Sample analysis times typically are short, ranging from 1 to approximately 10 min. Furthermore the techniques are such that they can often be made highly automatic. In situations where large numbers of similar samples are being routinely analyzed, the cost per sample may compare favorably therefore with other methods. If, in addition, multi-element analysis is needed for every sample and can be provided by a nuclear or ion beam technique, the cost per element per sample may turn out to be lower and on occasion even so much lower that one of these techniques may become the technique of choice because it is the least costly.

The low precision is due to statistical errors which are associated with counting random events and to calibration problems. Calibrations, achieved most commonly through comparison standards, require special attention because the measurement result depends not only on the quantity of an element present but also on the depth distribution of that element in the sample surface. The result depends on depth because reaction cross sections depend on energy and because the incident ion loses energy as it penetrates into the sample. Precisions range commonly from 1% to approximately 10%. Precisions as low as 0.1% have been reported (9,10) (for neutron activation analyses), but these are achieved only with the utmost care. Chapter 15 of Ref. 7 deals specifically with accuracy, precision, and standards.

It is worth mentioning that ion beams at keV energies can be used to produce accurate trace element standards, including the noble gases, through ion implantation (11). The number of implanted beam atoms is measured easily to a few percent or better through the integrated electrical charge which is deposited into the target. The sensitivity of the electrical measurement is such that amounts which are orders of magnitude below the sensitivity of the best chemical and physical analysis methods can be deposited quite accurately. The integrated charge can of course be controlled to produce whatever concentration is desired. The method is best suited to trace element standards but can, with appropriately long irradiations, be used also to achieve concentrations of a fraction of a percent.

It is convenient to divide the ion beam analysis techniques into two categories: activation analysis and prompt radiation analysis. Activation analysis with a charged particle beam is analogous to neutron activation analysis. The elements of interest in a sample are converted into radioactive species through nuclear reactions, and the characteristic radiations are measured after the irradiation. The half-life for decay frequently is used for identifying the isotope which is responsible for the radiation. Prompt radiation analysis is the term used when the instantaneously emitted radiations are detected; the radiations in this case can be due to either nuclear or nonnuclear reactions.

Charged particle activation analysis is included here for completeness but will be discussed only briefly. The major emphasis will be on prompt radiation analysis, a subject in which the most striking advances have recently been forthcoming.

II. CHARGED PARTICLE ACTIVATION ANALYSIS

A. Comments

In this method a stable element present in a sample is detected through the radioactivity produced as a result of nuclear reactions between that element and the irradiating beam. After irradiation, the sample containing the activated elements is placed in a low-background detector and the emitted radiations, usually gamma or beta rays, are measured. The sensitivity of the measurement is such that it is most commonly used for measuring elements which are present only in trace quantities. The trace elements which are to be measured may be present in the sample as extraneous impurities or they may be purposely introduced. The latter situation occurs, for example, when stable isotopes are used as tracers for studying some dynamic characteristic. Stable isotope tracers have the advantage that they can be used in many cases where the use of radioactive materials prior to analysis is precluded.

Although charged particle activation analysis is most commonly considered for trace element analysis, its possibilities for minor and even major constituent analysis should not be overlooked. This comment applies particularly well to surface analyses since the concentration of the detected element maybe at the major or minor constituent level in the surface even though it is at the trace level in the bulk of the sample.

An excellent discussion and a list of references for charged particle activation analysis has been given by Tilbury (3). Much interest has centered on ^{3}He particles since their advantages for activating the light elements were pointed out by Markowitz and Mahony (12). The proceedings from two series of conferences, one titled, "Practical Aspects of Activation Analysis with Charged Particles" (2,6), and one titled, "Modern Trends in Activation Analysis" (1,7), should be of particular interest because they contain descriptions of large numbers of specific examples. Another conference in the second series is scheduled to take place at the C.E.N. (Center d'Etudes de l'Energie Nucleaire), Saclay, France, in October of 1972; as before, proceedings of the conference will be published. Other useful reports on charged particle activation analysis maybe found in Refs. 12 through 24.

The charged bombarding particles which are of greatest interest for measuring gases in metals are protons, deuterons, and ^{3}He particles. Hydrogen and helium cannot practically be observed with activation analysis, although in principle the lithium ion beam

and other light element beams can produce radioactivities upon interaction with the nuclei of these two elements. Very little charged particle activation analysis work has been reported for the noble gases Ne, Ar, Kr, and Xe (25,26). If needed, charged particle activation analyses could very probably however be developed for these gases. The remaining gases N, O, F, and Cl have all been determined by charged particle activation analysis.

The problem of interferences from elements other than those whose determination is desired must be carefully considered for charged particle activation analysis just as is frequently the case for other techniques. That surface analyses are especially susceptible to contamination from the ambient atmosphere is well known.

Although the most efficient approach to a specific problem will usually be to consult the literature, the following general comments may be helpful. The magnitude of the cross section for a particular desired nuclear reaction will often be different from that of possible interfering reactions and in general will have a strongly different dependence on the energy of the incident ion. Both of these factors may be useful for minimizing or evaluating the contributions from interfering elements. Thus, for example, because of Coulomb barrier effects, as the bombarding energy is lowered the interference from higher Z (atomic number) elements typically is reduced relative to lower Z elements. An even simpler situation results if one of the interfering reactions in question has a negative Q value, or energy release. Such a reaction will not proceed at all until the incident beam energy exceeds an easily calculable threshold energy, and it is possible then, by irradiation at an energy below this value, to eliminate the interference from this reaction completely. Changing from one bombarding particle species to another will usually also result in different relative interferences such that an evaluation of the various interfering contributions may be made possible. The above comments are directed particularly at those situations where no chemical separations are performed on the sample, since this is judged to be desirable whenever possible. In practice, interfering radioactivities are oftentimes also removed by chemical separations.

The number and variety of samples which have been studied and reported upon in the literature are such that it may be possible for the reader to find discussions of problems which are similar, if not identical, to his own. Reference 26, with its comprehensive coverage and extensive cross indexing by subject, should prove particularly valuable for this purpose. As an introduction to the literature, a few selected articles are abstracted briefly in the sections which follow.

B. Examples of Applications

1. The application of ^{3}He-induced nuclear reactions to activation analysis for oxygen and other elements has been discussed in a short review article by Markowitz and Mahony (12). Analyses for oxygen were performed in beryllium, thorium, and Mylar samples through detection of the radioactive ^{18}F isotope produced by the ^{16}O(^{3}He,p) ^{18}F reaction; ^{18}F is a positron emitter with a 110-min. half-life. For a 1-μA beam of 7.5-MeV ^{3}He ions incident on a 0.0005-in. Al foil, an ultimate sensitivity of 1 part per billion (ppb) is estimated; for higher intensity beams and water-cooled target samples (to prevent melting) sensitivities of fractions of a part per billion are indicated. Actual analyses were performed with a 31-MeV ^{3}He beam from the Lawrence Radiation Laboratory's Hilac accelerator. Procedures for determining the overall detection efficiency are described. Precision and

accuracy are estimated to be ± 5 and ± 10%, respectively. Suggestions are made for evaluating possible interferences from sodium and fluorine as a result of the $^{23}Na(^{3}He,2\alpha)^{18}F$ and $^{19}F(^{3}He,\alpha)^{18}F$ reactions. For oxygen analysis in thorium, thin foils of thorium (0.001 in.) were mechanically cleaned and washed in nitrogen atmosphere, sealed in a 0.001-in. polystyrene envelope so that oxygen was excluded from the sample's surroundings, and irradiated and counted while in this envelope. The article also lists all of the common nuclear reactions of ^{3}He ions with nuclides from ^{6}Li through ^{48}Ca, along with product half-lives and reaction Q values.

The variation of the reaction cross section with energy, the same factor which can be useful in eliminating or evaluating interferences, complicates the problem of measuring the quantity of an element present in a sample. The reason for this is that the incident-beam ion loses energy as it penetrates into the sample and the magnitude of the cross section therefore is different at different positions along the penetration path. Some nuclear reactions exhibit such sharp "resonances," that is, increased cross sections at specific incident energies, that the reaction cross section can change by an order of magnitude if the beam ion energy changes by only a few hundred parts per million. Such reactions are important when prompt nuclear radiation measurements are made, but are not commonly used for charged particle activation analysis; these reactions will therefore not be treated here but will be discussed instead in the prompt radiation analysis section.

For nonresonant nuclear reactions the cross section changes relatively more slowly with energy. In this case, therefore, when the target thickness is small compared to the penetration range of the incident ion the reaction yield Y maybe written as

$$Y = n\,N\,\Delta x\,\sigma\,(E), \tag{1}$$

where

Y = the number of reactions produced
n = the number of incident beam particles
N = the number of reactant target atoms per cubic centimeters
Δx = target thickness in centimeters
E = incident particle energy
$\sigma(E)$ = reaction cross section in square centimeters at energy E.

If the target is thick the formula becomes

$$Y = n\,N \int_{O}^{E} \frac{\sigma(E')\ dE'}{\frac{dE'}{dx}(E')}, \tag{2}$$

where E′ is the variable energy of the incident particle as it penetrates into the target and

$$\frac{dE'}{dx}(E')$$

is the stopping power dE′/dx as a function of E′. For simplicity N is assumed to be uniform in the sample; if it is not, its depth distribution must also be taken into account under the integral sign in Eq. (2). Normally, the dependences of the cross section $\sigma(E')$ and the stopping power

$$\frac{dE'}{dx}(\text{and } E')$$

on E′ are obtained from experimental data or calculations (27) and are used to evaluate the integral over $\sigma(E')$.

2. Ricci and Hahn (15,16) have greatly simplified this calculation by introducing a thick target average cross section so defined that, once this cross section is evaluated, it is possible to use range energy data without integration to calculate the reaction yield. The two articles cited also contain discussions of measurement calibrations and other experimental procedures as well as extensive lists of sensitivities for activation analysis of elements from Be through Ca with 18-MeV ^{3}He particles. The sensitivities for nitrogen and oxygen are among the highest. On a relative scale the sensitivities listed for nitrogen, oxygen, fluorine, and chlorine, respectively, are 725, 704, 114, and 11. The corresponding reactions and product half-lives are $^{14}N(^{3}He,d)^{15}0$, 2.07 min; $^{16}O(^{3}He,p)^{18}F$, 110 min; $^{19}F(^{3}He,\alpha)^{18}F$, 110 min; and $^{35}Cl(^{3}He,\alpha)^{34m}Cl$, 32.4 min. The notation ^{34m}Cl signifies that the product radioactive nucleus has been left in a metastable state. The radiation from this state, which decays with a 32.4-min half-life, is more convenient to measure than that from the ground state of ^{34}Cl, which has a half-life of 1.5 sec.

3. Deuteron activation analysis has been used for analysis of C, N, and O contamination of high-purity metallic surfaces by R. W. Benjamin and others (17). The energy of the deuterons used was 2.6 MeV and the metals analyzed were beryllium, molybdenum, and tungsten. A particularly interesting technique was that in which a vacuum chamber for the irradiations was separated from the Van de Graaff accelerator vacuum system by a 0.0001-in.-thick molybdenum foil to avoid carbon contamination. The reactions used and the corresponding product half-lives were $^{12}C(d,n)^{13}N$, 9.96 min; $^{14}N(d,n)^{15}O$, 2.07 min; and $^{16}O(d,n)^{17}F$, 1.1 min. The authors found that the relatively long ^{13}N half-life makes the carbon analysis insensitive to the presence of oxygen and nitrogen. The detection limits for nitrogen and oxygen, however, depend on the concentrations of the other two impurities. Achievable detection limits were estimated to be 1 ppm for carbon, 2 ppm for oxygen, and 5 to 10 ppm for nitrogen.

4. Debrun, Barrandon, and Albert (18) have investigated the determination of carbon, oxygen, and sulfur in high-purity iron, nickel, and chromium samples by irradiation with ^{3}He and ^{4}He particles. Interferences from nitrogen, sodium, magnesium, and fluorine are discussed. While interference from the first three elements can be satisfactorily limited by lowering bombarding energy, that from fluorine cannot be so eliminated. The ratios of fluorine to oxygen production cross sections for radioactive ^{18}F were therefore studied as a function of energy for both ^{3}He and ^{4}He particles. In the case of ^{3}He irradiations, the ^{18}F contribution per atom from fluorine is shown to be less than 8% of that from oxygen. Reactions interfering with carbon and sulfur determinations were investigated, and data for a number of interference ratios are presented. Activation analyses by irradiation with deuterons and protons are also discussed.

5. Tritons can be used to analyze for oxygen in the presence of fluorine because they do not induce any radioactivity which can interfere with the ^{18}F produced by the $^{16}O(t,n)^{18}F$ reaction. A compact discussion of the use of tritons for oxygen analysis in metal surfaces has been given by Barrandon and Albert (19). Excitation functions in the energy range from 0.5 to 3.0 MeV are presented. The investigations included a study of the variation of surface oxygen on pure zirconium and aluminum as a function of chemical and mechanical polishing. The method can be used, with no chemical separations being necessary, for aluminum, iron, chromium, nickel, and zirconium. Sensitivities lie in the range from 100 to 10^{-3} $\mu g/cm^2$.

6. Activation analyses for oxygen and carbon on the surfaces of highly purified gold and platinum have been reported by Butler and Wolicki (22). Of particular interest are the tests made to determine whether contaminants were introduced onto the target surfaces from the accelerator vacuum system. These tests showed that carbon contamination could be kept below 10^{-2} atomic layers for the duration of an irradiation by surrounding the target as completely as possible with trapping surfaces at liquid nitrogen temperature. One atomic layer is defined simply as $N^{2/3}$, where N is the number of host material atoms per cubic centimeter. Ultimate sensitivities for oxygen and carbon are estimated to be 10^{-3} and 10^{-4} atomic layers, respectively. The reactions used were $^{16}O(^{3}He,p)^{18}F$ and $^{12}C(^{3}He,\alpha)^{11}C$, respectively.

7. The $^{37}Cl(d,p)^{38}Cl$ reaction has been used by Knudson and Dunning (24) to detect trace amounts of chlorine on aluminum. The sample was bombarded with 5.0-MeV deuterons and the resulting gamma ray activity was measured with a 5-in.-diameter by 5-in.-thick well-type NaI(Tl) scintillation detector. Carbon, nitrogen, and oxygen did not present any interference to the observation of ^{38}Cl. Measurements on 125-μm-thick commercial aluminum foil indicated considerable interference with the chlorine gamma-ray spectrum as observed with a NaI(Tl) detector. Later measurements with a high-resolution Ge(Li) solid-state detector showed that the interference was caused by the presence of manganese and gallium in the commercial foils. Radioactive ^{28}Al, produced by the $^{27}Al(d,p)^{28}Al$ reaction, could interfere with the ^{38}Cl. Fortunately, however, because the 2.27-min half-life of ^{28}Al is much shorter than the 37.2-min half-life of ^{38}Cl, counting can be delayed until the ^{28}Al activity has decayed to a tolerable level. A sensitivity of 0.2 $\mu g/cm^2$ was estimated. A substantially higher sensitivity should be achievable for chlorine on high-purity, high-Z metals.

8. An interesting application of charged particle activation analysis has been described by Holm, Basmajian, and Sanders (28). In that work the microscopic distribution of oxygen and carbon in metals was observed by bombardment of metallographically polished samples with 6.5-MeV ^{3}He ion and autoradiography of the activated areas. Positional resolution of 13 μm was obtained in samples having bulk carbon concentrations of about 250 ppm.

9. Dynamic processes can be studied through the use of stable isotope tracers and subsequent charged particle activation analysis. Ritter and others (29) and more recently Carosella and Comas (30) have used enriched ^{18}O to study the oxidation of silicon single crystals. The amounts of ^{18}O present on the sample surface after various exposures of the sample were measured through the $^{18}O(p,n)^{18}F$ reaction. The sensitivity of the method was such that oxide layers as thin as 0.01 atomic layers were measurable.

III. PROMPT RADIATION ANALYSIS

In this method the presence of an element in a sample is detected through the radiation which is emitted instantaneously when the incident beam ion interacts with an atom of that element. Detection limits can be quite good; typically they are not as good, however, as can be achieved under ideal conditions with charged particle activation analysis. Chemical separations are precluded although, of course, prompt radiation analysis can be performed on chemically separated sample constituents. Specificity and accuracy of prompt radiation analysis can be high; precision suffers from the same statistical counting limitations and calibration difficulties that were mentioned earlier. Even though chemical

separations are not possible, the problem of interferences is sometimes simpler to solve for the case of prompt radiation analysis than for charged particle activation analysis because of the greater diversity of reactions and reaction types which can be considered for a specific problem.

The reaction between the two interacting atoms can be either nonnuclear or nuclear. The two principal examples of nonnuclear reactions induced by positive ion beams are elastic scattering and atomic excitation or ionization. Strictly speaking, if the incident ion energy is greater than or comparable to the Coulomb barrier energy for the interaction, then nuclear reactions can contribute to elastic scattering. For simplicity, elastic scattering will, however, be considered here as nonnuclear in origin; effects due to nuclear interactions can always be taken into account through the use of the experimentally measured elastic scattering cross sections for the atoms and energies in question.

In elastic scattering, the incident beam ion is scattered from an atom in the sample by a collision in which energy and momentum are both conserved. For a fixed incident energy and scattering angle the energy of the scattered beam ion depends on the mass of the struck atom and can be used therefore to identify that mass. The characteristic radiations from excited or ionized atoms in solids which are most useful for analysis are the x rays. In distinction to nuclear reactions, which typically allow analysis for a few elements at most in a single irradiation, elastic scattering and ion-induced x rays can often be used to measure a large number of elements in one irradiation.

Nuclear reactions may be categorized according to three basic mechanisms, each of which may exhibit either resonant or nonresonant dependence on the incident particle energy. The first of these is the simple capture of the incident particle by the struck nucleus to form a compound nucleus which then decays by the emission of a charged particle or one or more gamma rays. The second is the inelastic scattering of the incident particle, part of the incident energy being absorbed by the struck nucleus which is then left in an excited state. The third mechanism is that of rearrangement collisions. This term is applied to all reactions in which the particles which separate after a collision are different from those which entered into the collision. For many reactions, in all three of the above categories, the emitted radiations have discrete and well-defined energies characteristic of the reaction which has occurred between the incident and the struck nuclei. Therefore, these radiations can be used to identify the nuclear species and, therefrom, the chemical elements in a sample which is being irradiated.

An important advantage of prompt radiation analysis is that information can be obtained about the depth distribution of elements near the sample surface. The dependence of prompt radiation characteristics on depth results from the energy losses suffered by incident ions as they penetrate into the sample, and, in the case of the emitted radiation being ionized particles, also from the energy losses suffered by these particles as they emerge from within the sample. Etching and other surface removal techniques are sometimes used for depth distribution measurements, but these are laborious and often do not approach the resolution possible with prompt radiation analysis. Nuclear resonant reactions are especially powerful in this regard.

Another advantage of prompt radiation analysis is that spatial information in the plane of the surface can be obtained about chemical composition, the spatial resolution of such measurements being determined by the diameter of the incident ion beam. The pioneering work of the Harwell Laboratories on the use of small-diameter beams for

microprobe analysis deserves particular mention. Most recently Cookson and Pilling (31) have developed a 3-MeV, 6-nA, proton beam less than 4 μm in diameter. Pierce (32) has discussed the analysis of samples which utilizes a scanning of this beam across the sample either mechanically or by electrostatic beam deflection. The need for spatial information about elemental composition in the plane of the surface will undoubtedly spur additional work and development in this area.

For the various categories of prompt radiation analysis reactions, a general description of the reaction characteristics and experimental techniques will be followed by examples of actual applications of a given technique. Whenever possible examples will be discussed which pertain to the problems of gases in metals. The existing literature on prompt radiation analysis is, however, rather more limited than was the case for charged particle activation analysis. To show adequately how the various techniques are applied, examples dealing with elements other than gases and metals have had to be used. Reference 26, a cross-indexed, activation analysis bibliography, should again be useful for consulting the literature. The proceedings for the four charged particle activation analysis conferences (1,2,6,7) also contain a number of articles that discuss prompt radiation analysis applications.

A very interesting physical phenomenon called *channeling* is the basis of a powerful technique for analyzing single crystals. This technique, which depends on accurate alignment of an incident, well-collimated beam with one of the low-index or close-packed crystal axes, can utilize, as appropriate, any one of the types of ion beam interactions being considered here. Channeling can under proper conditions give information not only about elemental composition but also about the substitutional or interstitial character of a chemical impurity. It also provides a sensitive measurement of crystal surface disorder. This technique will be discussed in the elastic scattering section since, most channeling measurements are performed by this type of reaction. It is interesting to note that when the beam diameter is small compared to the grain size it should, in principle at least, be possible to perform channeling measurements on the individual crystals of a polycrystalline material such as a metal.

A. Elastic Scattering Reactions

The application of elastic scattering to elemental surface analysis was discussed in 1957 in an excellent article by S. Rubin and others (33). In a famous experiment, Turkevich, Franzgrote, and Patterson used alpha-particle backscattering to perform the first direct chemical analysis of the moon (34). (Later, chemical analyses on lunar matter brought back to earth by the Apollo 11 mission showed excellent agreement with the elastic scattering measurements.) A useful review of the principles involved in elastic scattering experiments has been given also by Anders (35). Other contributions to this subject area maybe found in Refs. 36 through 52.

In the past few years the elastic scattering technique has received a great deal of interest. It has been improved in mass and depth resolution and has been applied at energies ranging from 0.5 keV to 10 MeV and above and used with beam ion masses ranging from the proton to ^{40}Ar and above. The references cited contain more detailed discussions of the principles which apply to the elastic scattering mechanism than can be included here. The following brief introduction to the subject may, however, be useful; additional details will be given in the examples which will be discussed.

An elastic scattering event is, first of all, a collision between two particles in which energy and momentum are both conserved. For such a collision the following relation may easily be derived for the energy E of the scattered (beam) ion

$$E = E_0 \frac{{m_1}^2}{(m_1 + m_2)^2} \left[\cos\theta + \left(\frac{{m_2}^2}{{m_1}^2} - \sin^2\theta \right)^{1/2} \right]^2, \tag{3}$$

where

E_0 = incident beam ion energy
m_1 = mass of the incident ion
m_2 = mass of the struck atom
θ = angle of scattering as measured to the incident direction.

This equation shows that for a fixed angle of detection, the energy of the scattered ion depends on the mass of the scattering atom. Conversely, if the scattered energy spectrum is measured, Eq. (3) may be used to calculate the various masses present in the sample.

For targets which are thin compared to the penetration range of the incident beam, the number of particles S scattered by atoms of mass m_2 into solid angle Ω is given by

$$S = n\, N(m_2)\Delta x \Omega \sigma(E_0,\theta,m_1,Z_1,m_2,Z_2), \tag{4}$$

where

n = number of incident beam atoms
$N(m_2)$ = number of scattering atoms of mass m_2 per cm^3
Δx = target thickness in cms
Z_1 = atomic number of incident atoms
Z_2 = atomic number of scattering atoms
σ = elastic scattering cross section in cm^2/sr.

At incident energies below a few MeV and above about 50 keV, the elastic scattering cross section is usually purely Rutherford and is given by

$$\sigma_R = \frac{{Z_1}^2\, {Z_2}^2\, e^4}{16\, E_0^2} \times (k+1)^2 \csc^4\left(\frac{\varphi}{2}\right) \times W(k,\theta), \tag{5}$$

where

e = electronic charge

$$k = \frac{m_1}{m_2}$$

$$\varphi = [\theta + \sin^{-1}(k \sin\theta)] = \text{scattering angle in the center of mass system} \tag{6}$$

$$W(k,\theta) = \frac{[k\cos\theta + (1 - k^2 \sin^2\theta)^{1/2}]^2}{[1 - k^2 \sin^2\theta]^{1/2}}. \tag{7}$$

Values of σ_R calculated from these equations are given in millibarns (10^{-27} cm^2) per steradian in Table 1 for the example E_0 = 3.0 MeV, θ = 165°, m_1 = 4, and Z_1 = 2. When the scattering is not Rutherford, the appropriate experimental or calculated cross section must be used in Eq. (4). The number of beam particles n is usually measured as the integrated charge incident on the target; the detector solid angle is a constant for a particular experimental arrangement and can also easily be measured. A measurement of S can yield therefore $N(m_2)\Delta x$, the number of scattering atoms of mass m_2 per square centimeter, or, if Δx is known, $N(m_2)$ the number of such atoms per cubic centimeter. Frequently, as is done in other methods also, the simplest and most practical way to obtain $N(m_2)\Delta x$ is to perform a comparison measurement with a standard sample for which this quantity is known.

Table 1
Values of E, E/E_0 and the Rutherford Scattering Cross Section σ_R Calculated for E_0 = 3.0 MeV, m_1 = 4, Z_1 = 2, and θ = 165°

Element	m_2	E(MeV)	E/E_0	σ_R(mb/sr)
Pb	208	2.781	0.927	4005
Au	197	2.770	0.923	3716
W	184	2.754	0.918	3261
Ce	144	2.690	0.897	2002
Xe	129	2.656	0.885	1735
Ag	109	2.597	0.866	1313
Mo	96	2.546	0.849	1048
Kr	84	2.487	0.829	769.2
Zn	66	2.363	0.788	532.7
Ni	60	2.307	0.769	463.3
Fe	56	2.264	0.755	399.0
Cr	52	2.216	0.739	339.5
Ti	48	2.160	0.720	284.7
Ca	40	2.022	0.674	233.9
Cl	37	1.958	0.653	168.4
Cl	35	1.910	0.637	167.9
S	32	1.830	0.610	148.0
P	31	1.801	0.600	129.8
Si	28	1.704	0.568	112.3
Al	27	1.668	0.556	96.5
Mg	25	1.590	0.530	81.6
Na	23	1.503	0.501	68.0
Ne	22	1.456	0.485	55.9
Ne	20	1.352	0.451	55.1
F	19	1.294	0.431	44.2
O	16	1.098	0.366	33.7
N	14	0.944	0.315	24.8
C	12	0.767	0.256	17.1
B	11	0.670	0.223	11.32
Be	9	0.457	0.152	6.22
Li	7	0.232	0.077	2.49

In principle, for very thin targets, well-defined beam energy, and high-resolution detection systems, it should be possible to identify all masses in the target differing by at least one atomic mass unit, each scattering mass being observed as a sharp peak in the energy spectrum of the scattered particles. The mass resolution of the measurement depends on the narrowness of the observed peaks which in turn depends on the incident beam energy spread, the detector solid angle subtended, the intrinsic detector system resolution, and the target thickness. Typically, beam energy spread is small (a few parts per thousand or less) because most accelerator beams are magnetically analyzed before they strike the target. Therefore, resolution is most often determined by target thickness and detector system resolution. The subtended solid angle affects resolution simply because the backscattered energy changes with the angle of scattering. The peak broadening produced by this effect is commonly termed *reaction kinematic broadening* or sometimes just *kinematic broadening.* This term is applied also to the spectra of particles emitted from nuclear reactions. Detector resolutions of about 15 keV are conveniently obtainable with commercially available, solid-state detectors. If resolutions significantly better than this value are desired, resort must be made to magnetic or electrostatic analyses of the charged particles being detected. However, the backscattering technique is subject to a basic ambiguity in the case of targets sufficiently thick so that the beam particles can lose appreciable energy before the scattering event takes place; the corresponding scattered particles then also lose energy as they emerge from the target. In such cases it is not possible to distinguish between a scattering from a light atom close to the surface and a scattering from a heavy element deeper in the target.

In practice, for thin targets and solid-state detectors, it is possible to resolve peaks in the energy spectrum that are about 60 keV apart. The mass resolution corresponding to this value can be estimated from Table 1, which shows the energy calculated from Eq. (3) that a 3.0-MeV alpha particle possesses after scattering through an angle of 165° from various masses. Mass resolution in percent improves for a given incident particle and scattering angle as the scattering mass decreases. The column labeled E/E_0 can be used for calculating the energy E for other values of E_0, since the fraction of energy lost in a scattering does not depend on the incident energy. It is easy to see from this column that the scattered energy difference between the peaks corresponding to two given scattering masses increases as the incident energy increases; mass resolution therefore will be better at higher energies, all other factors being equal.

Because mass and depth resolution in general are better at large or backward scattering angles than at forward angles, most experiments are performed in a "backscattering" geometry. The arrow labeled *beam particles* in Fig. 1 corresponds, for example, to a backscattering event. The example discussed in the following section is of this type. Included in the list of examples are experiments on high- and low-energy backscattering, channeling, and forward scattering coincidence measurements. The discussions emphasize the measurement technique itself; the results of the various experiments are considered only to the extent that they display the potentialities of the scattering measurements.

1. *High-Energy Backscattering* — A number of interesting features of the backscattering technique can be illustrated by the results obtained recently by Hirvonen, Weisenberger, Westmoreland, and Meussner (52) in an experiment which utilized a relatively simple geometry. Thin films of chromium and gold were deposited on 1-mm-thick sapphire substrates, and the 165° scattering of 3-MeV alpha particles was used to study the migration of the chromium as a function of annealing temperature. Figure 2 shows schematically the geometry of the experiment. Alpha particles of 3.0 MeV energy were obtained

from a Van de Graaff accelerator and were detected, after scattering, by a surface barrier detector whose resolution was less than 15 keV full width at half maximum. The energy spread in the beam was approximately 3 keV.

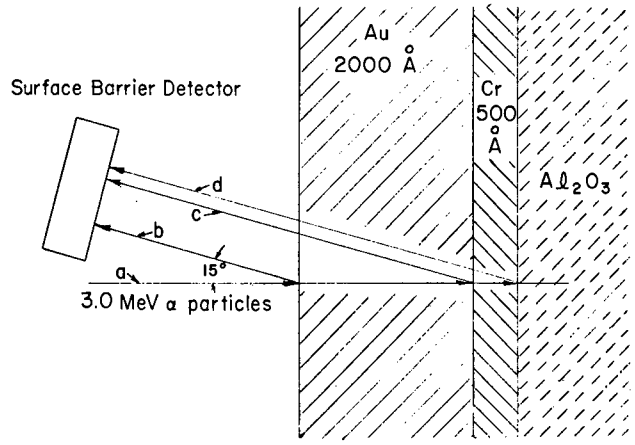

Fig. 2 — The backscattering of Alpha particles from thin films of Cr and Au on a sapphire substrate

Figure 3 shows the data obtained with chromium and gold film thicknesses of 500 and 2000 Å, respectively. The lower part of the figure shows the energy spectrum of the scattered alpha particles as obtained before annealing. Reference to the rays *a*, *b*, *c*, and *d* in Fig. 2 will be helpful toward explaining the features of this spectrum. First of all, path *ab* represents scattering from the topmost surface of the gold. For this path the scattered alpha particle loses energy only in the elastic collision with a gold atom and arrives at the detector with an energy (see Table 1) of $E_{ab}(Au) = 0.923\ E_0 = 2.770$ MeV. The high-energy side of the gold peak in Fig. 3 corresponds to path *ab*. For scattering events beneath the surface the alpha particle loses energy both on the way in, and, after scattering, on the way out. The low-energy side of the gold peak in Fig. 3 corresponds to path *ac*, that is, to a scattering from a gold atom at the gold—chromium interface. If the assumption is made that the energy loss of the alpha particle per centimeter of path in gold does not change rapidly with energy, the minimum energy on the low-energy side of the gold peak will be given by

$$E_{ac}(Au) = 0.923\ [E_0 - \Delta E(Au)] - \sec 15^\circ\ \Delta E(Au), \qquad (8)$$

where $\Delta E(Au)$ = the energy lost by the alpha particle in traversing the full thickness of the gold film. (In practice, for best accuracy, account should be taken of the fact that the energy loss per centimeter of path does change with energy.) For scattering points intermediate between the front and back surfaces of the gold, the alpha particle will arrive at the detector with energies between 2.770 MeV and $E_{ac}(Au)$, thus giving rise to a broad peak whose energy width is related to the thickness of the gold film from which the scattering is taking place. The total area under the peak is related to the total number of gold atoms per square centimeter ($N(m_2)\Delta x$ in Eq. (4)) which the beam traverses.

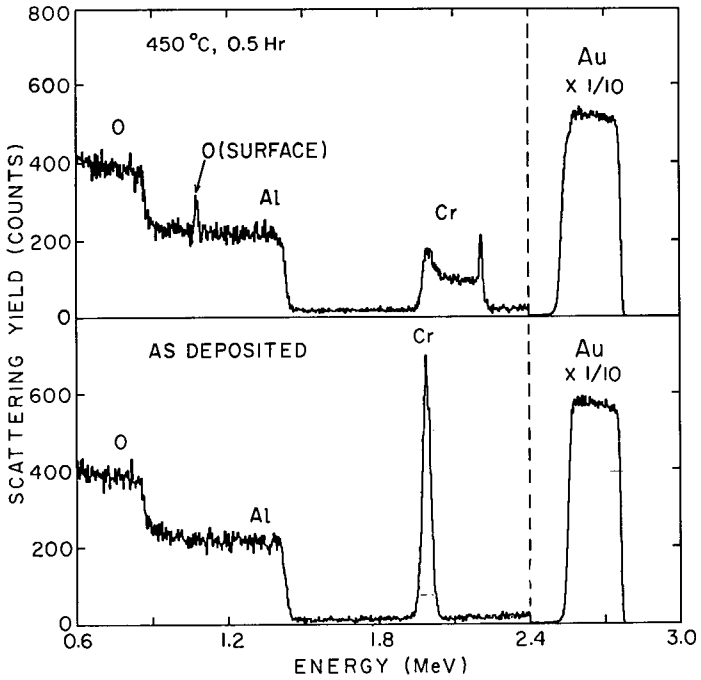

Fig. 3 — Alpha particle scattering yield at 165° from a Au-Cr-Al_2O_3 target before and after anneal (submitted to Appl. Phys. Lett.; used by permission of the American Institute of Physics)

Similar considerations show that the maximum energy on the high-energy side of the chromium peak corresponds to an alpha particle which has scattered from the front-most surface of the chromium layer, and has traveled along path *ac* to the detector. This energy is given by

$$E_{ac}\ (Cr) = 0.739\ [E_0 - \Delta E(Au)] - \sec 15^\circ\ \Delta E(Au). \quad (9)$$

The minimum energy on the low-energy side corresponds then to an alpha particle which has scattered from the back surface of the chromium layer and has traveled along path *ad* to the detector. This energy is given by

$$E_{ad}\ (Cr) = 0.739\ [E_0 - \Delta E(Au) - \Delta E(Cr)] - \sec 15^\circ\ [\Delta E(Au) + \Delta E(Cr)], \quad (10)$$

where $\Delta E(Cr)$ is the energy loss in the Cr film. The fact that the observed chromium peak does not exhibit a flat top implies that the energy difference $E_{ac}(Cr) - E_{ad}(Cr)$ is less than or equal to the energy resolution of the detection system. Again, the area under the peak gives the number of Cr atoms per square centimeter traversed by the beam.

Finally, the plateaus labeled Al and O result because the sapphire substrate is thicker than the penetration range of the incident alpha particles. The sharp rises or steps at approximately 1.45 and 0.89 MeV correspond to scattering along path *ad* from Al and O, respectively.

The upper portion of Fig. 3 shows the results obtained after the sample had been subjected to a one-half hour anneal in argon at 450°C. (This sample had also previously received a number of heat treatments at 150°C and 250°C; at 250°C only a relatively

small amount of diffusion was observed.) The Cr peak has first of all broadened toward higher energies. The narrow peak on the high-energy side of the Cr now corresponds to scattering from Cr along path *ab* in Fig. 2, that is, to Cr which is situated at the front surface of the gold. This peak shows clearly that, for these conditions of anneal, the Cr has migrated through the Au film and has built up in concentration at the surface. The flat "valley" portion of the Cr broad peak corresponds to a distribution of Cr throughout the rest of the Au layer which is approximately uniform. It is important to note that the elastic scattering measurement performs an average over the beam spot area and cannot distinguish within this area between a homogeneous distribution of Cr in the gold and a nonuniform distribution consisting, for example, of thin Cr filaments having the same averaged density. The peak labeled O (surface) corresponds in energy to oxygen which is now present at the front surface of the sample, present there presumably because of the oxidation of the Cr which has reached this surface. The change in shape of the rear edge of the Au peak indicates interdiffusion of the Au and the Cr at the previously well-defined Au-Cr interface. It is of interest also to note that peak shapes can be different for the case when one interface element is predominantly diffusing into another, from those obtained when the two elements are diffusing equally into each other.

The qualitative features of the curves in the upper portion of Fig. 3 can be converted into quantitative depth distributions of elemental concentrations if the energy loss per centimeter of the incident and outgoing particles is known in the target. The reason for this is that it is then possible to convert observed energies to depths and observed energy intervals to layer thicknesses Δx. Counts per unit energy interval are used instead of peak areas to obtain the number of atoms of mass m_2 per cm^3 i.e. $N(m_2)$, at a given depth. It should be noted, however, that the conversion of the energy scale along the abscissa to a depth scale in the target depends on the mass from which the scattering is taking place, so it is necessary to correct for this dependence both in calculating the depth which corresponds to a given energy in the spectrum and in calculating the layer thickness Δx which corresponds to a given energy interval in the observed spectrum.

When the ratio of two elemental concentrations is desired, the situation simplifies somewhat in that the ratio depends less strongly on an accurate knowledge of the stopping power of the sample than do the individual concentrations. Thus, for example, the depth distribution of the stoichiometry of the aluminum oxide substrate could be estimated (if it were not known) from the heights of the Al and O "steps" in Fig. 3 to a better accuracy than that to which the stopping power for this material is known. For targets from 300 to 2000 Å thick, Meyer, Gyulai, and Mayer (40) and Mitchell, Kamoshida, and Mayer (41) discuss a method which can measure the ratio of the concentrations of two elements to good accuracy even if the stopping power for the material is not known. The method utilizes the energy widths of the observed peaks to obtain a ratio of depth scales in the sample.

Picraux and Vook (44) have discussed multilayer thin-film analysis for Er, Sc, or V layers, 500 to 2000 Å thick, on Kovar or sapphire substrates. One particularly useful observation made by these authors is that interfacial diffusion at an upper surface, that is, one closer to the front surface of the target, will not decrease the sharpness of the energy edges due to lower interfaces, whereas upper film thickness nonuniformities will contribute directly to the lack of sharpness of the energy edges of lower interfaces. The article also treats the case when a narrow overlap between two broad peaks in the energy spectrum gives rise to a narrow peak in the region of overlap. The sharpness or lack thereof of this overlap peak also can be used to obtain information on interfacial diffusion.

In the case of thick targets, Eq. (4) must be restated in an integral form similar to that of Eq. (2). In practice, however, the need for integration can frequently be avoided through the use of simplifying approximations regarding target composition and the dependence of the energy loss on energy and on target composition. The ambiguity, mentioned earlier, between light elements close to the surface and heavy elements in deeper, cannot however be simply overcome. Similarly, a measurement on a given element cannot be performed if the corresponding backscattering results cannot be resolved from the rest of the spectrum. Outside of these two constraints, extensions of the measurements from the simple sample discussed here to more complex samples should be possible; again, Refs. 36 to 52 should prove useful for this purpose.

Proton and helium backscattering measurements have been carefully investigated at 100 keV by Buck and Wheatley (50). This energy is interesting because the ion accelerator required is much less expensive than those which produce MeV energies. The authors cited have shown that the scattering at this energy is essentially Rutherford and that the sputtering away of metal target surfaces is negligible. Because the penetration range at 100 keV is small, this technique samples a thinner surface layer than higher energy experiments. This can be an advantage in that it can in some cases reduce the interfering background from the bulk of the sample. The penetration range is not so short as to be greatly affected by monolayer films so, in common with higher energy measurements, the technique does not require ultrahigh-vacuum techniques.

The method was used to detect surface impurities on silicon and graphite. A mass resolution of better than one unit in the low-Z region around oxygen and carbon was obtained through the use of a small cylindrical electrostatic analyzer in front of a solid-state detector. The electrostatic analyzer introduced the complication that it does not transmit neutral particles. Since charge neutralization is not negligible for 100-keV protons and He^+ particles moving in matter, a correction for this effect must be made.

2. *Channeling* — Thus far backscattering has been described for amorphous or polycrystalline materials. When the material being bombarded is a single crystal and when the beam is collimated so that its angular divergence is on the order of 0.1 degrees or so, an interesting phenomenon can be observed which has implications for backscattering measurements. This phenomenon, which is called channeling, is evidenced by a large decrease in the yield from any reaction which requires a close (about 0.2 Å) interaction between the beam atom and the target atom, when one of the close-packed or low-index symmetry axes of the crystal is aligned closely with the incident beam direction. Typically the yield can decrease by factors of 20 to 50. High-energy backscattering is a close-interaction reaction, so also are ion-induced x-ray production and inner shell ionization, and nuclear reactions.

For simplicity, channeling will be discussed in succeeding sections in terms of backscattering only; however, it should be understood that similar remarks will obtain for the other close-interaction reactions. In the channeling mode, just as in ordinary backscattering and subject to the same constraints, measurements can be made on a desired element through observations on the corresponding peak or structure in the backscattered energy spectrum; thus, measurements are frequently possible on either the host crystal elements or on impurity elements or both.

To see how a reduced probability for close interaction reactions can result when the beam is incident on a single crystal along a low-index direction, consider the schematic

diagram shown in Fig. 4. A single crystal target is shown in cross section with the atoms located on a square array having spacing d. For convenience the crystal is shown in fixed position and beam rays A through C are shown at various angles of incidence with respect to the crystal; in practice, the beam direction is fixed in space and the crystal is rotated to the desired orientation.

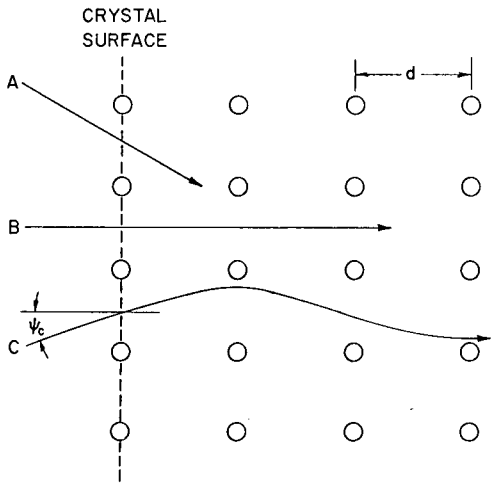

Fig. 4 — A schematic diagram showing ion beams incident on a single crystal for three different inclinations relative to the crystal axes

First of all, Ray A enters along a random direction into the crystal; the probability for a close interaction with an atom is therefore the same as it would be if the target were amorphous. The backscattering spectrum corresponding to Ray A incident on a thick crystal is shown schematically in Fig. 5. The increase in yield at lower energies is partly due to the inverse dependence of the Rutherford cross section on energy.

Ray B in Fig. 4 is aligned exactly with an atom row or plane. It is shown entering midway between two rows of atoms, but the entry points will in actuality be distributed uniformly over the crystal surface. Ray B will have a significant probability of undergoing a backscattering only if it enters the crystal at a point which is within approximately 0.2 Å of a surface atom center. Projected area considerations show that this should happen only about 2% of the time. In the ideal aligned case the backscattering yield might be expected to decrease by a factor of about 50. In actuality, lattice vibrations, crystal imperfections, etc., combine to decrease this factor somewhat. Ray B gives rise to the reduced intensity spectrum labeled in Fig. 5 as the aligned spectrum. The increase in intensity of this curve at lower energies reflects the increasing dechanneling of the beam as it penetrates into the crystal.

A beam need not enter at 0° to the surface normal, as does Ray B, in order to become channeled. As long as the momentum transverse to the crystal atom row is smaller than that required for approaching an atom site to within about 0.2 Å, the beam ion will suffer only small angle deflections and will not be scattered out of the channel. There is

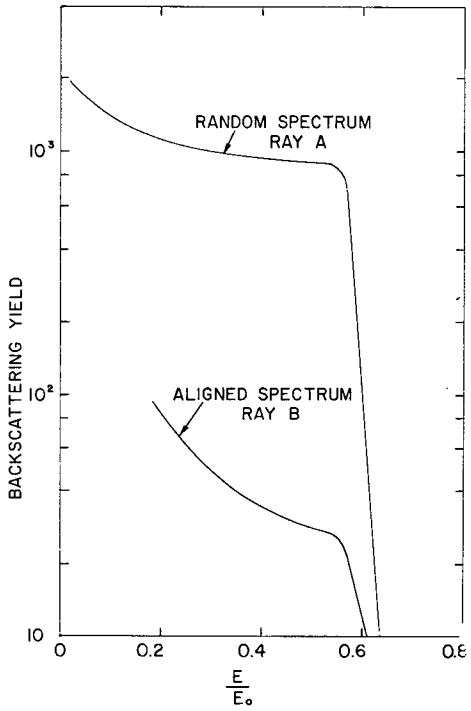

Fig. 5 — Schematic backscattering spectrum corresponding to rays A and B incident on a crystal along random and aligned directions, respectively

a calculable critical angle below which the beam will be channeled and show low yield for backscattering and beyond which it will undergo backscattering reactions and approach the random direction yield. Ray C is shown schematically at the critical angle. In practice the transition through the critical angle is not sharp, the critical angle being measured as the half-width of the yield curve at the point where the yield is half that of the difference between the random yield and the minimum yield. Figure 6 shows a backscattering yield curve as a function of angle of incidence, which was obtained by J. U. Andersen (53) for 0.5-MeV protons on single crystal tungsten; 0° incidence is parallel to the ⟨100⟩ crystal axis. The critical angle in this case was measured to be 1.68°, and the yield at minimum was down by approximately a factor of 40 from the random yield.

If one of the atoms in Fig. 4 is displaced by more than approximately 0.2 Å from its lattice site, it is, clearly, exposed to close interactions with an aligned beam. The decrease in backscattering yield occurs therefore only for atoms that are located on crystal lattice sites; backscattering from atoms which are interstitial, or which are present in thin amorphous surface films, is not affected. This means that if the host crystal lattice is presenting a background problem in the detection of a given interstitial or surface film element, alignment of the crystal so that the channeling mode is achieved can greatly reduce this problem. In consequence, a much higher sensitivity for detection of that element can be obtained than can be achieved if the entire sample is amorphous or polycrystalline (40).

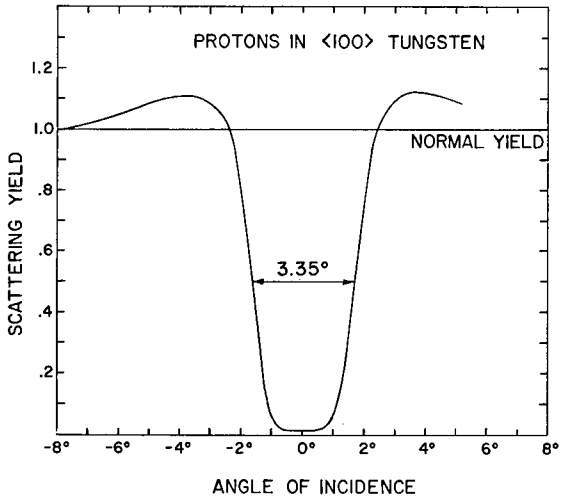

Fig. 6 — Backscattering yield of protons as a function of angle of incidence relative to the ⟨100⟩ axis of single crystal tungsten (Ref. 53)

The minimum backscattering yield from the crystal elements is strongly dependent on the perfection of the crystal, that is, on the extent to which all reactant atoms are in their proper lattice locations. Through this dependence, channeling has been used to study crystal structure imperfections (54-63).

Impurity atoms in a crystal can be either substitutional or interstitial. If they are substitutional, the backscattering yield from the impurity atoms will show a decrease in yield similar to that from the host crystal element. If the impurity atoms are interstitial the backscattering yield will usually show no dependence on the angle of incidence. Sometimes an interstitial atom lies accurately in one or two crystal atom planes. In such case, backscattering measurements for several different channeling directions can be used to triangulate on the impurity atom's location in the lattice (61-63). More usually, impurity atoms are only partly substitutional; the factor by which the random yield decreases can be used to determine what fraction is so situated (61-64). The atomic concentration of impurity atoms must be about 10^{-4} or greater before channeling measurements can be applied to such atoms (65).

Channeling has been of great interest to solid-state physics and particularly to the field of semiconductors. The references listed here constitute merely an introduction to the existing literature. Excellent survey articles on channeling have been prepared by Gibson (66) and by Davies (67). Much discussion pertinent to this subject may be found also in several conference proceedings (68-70) and in a book entitled, *Ion Implantation in Semiconductors*, written by Mayer, Eriksson, and Davies (71).

As an example, oxide and nitride films on silicon and gallium arsenide single crystals have been studied by channeling and backscattering measurements (40-42,72,73). In the case of silicon (40), measurements were made on the stoichiometry of the films as a function of distance from the interface between the bulk silicon and the surface films. The decrease in the aligned backscattering spectrum was used to reduce the silicon background under the oxygen and nitrogen peaks and thereby to improve the accuracy of the measurements. The ions used were 1- to 2-MeV ^{4}He. The energy resolution of the

surface barrier detectors which were used provided a depth resolution of between 100 and 150 Å. Film thicknesses studied ranged from 400 to about 2000 Å. Stoichiometry profiles obtained with backscattering alone gave good agreement with measurements which combined surface etching and backscattering. For gallium arsenide, backscattering and channeling were used to measure outdiffusion through silicon oxide and silicon nitride layers for various annealing conditions. Clear evidence was obtained for diffusion of gallium and for its accumulation at the surface of Si_3N_4 or SiO_2 layers on GaAs substrates after anneals at 700 to 800°C.

In still another interesting set of experiments, Matzke, Davies, and Johansson (64) used channeling combined with both backscattering and nuclear reactions to study the location of excess oxygen in the fluorite crystal structure of UO_2. During oxidation of UO_2 the structure remains unchanged until a composition of U_4O_9 is reached; further excess oxygen produces a phase change to the tetragonal structure U_3O_7. Therefore, experiments were performed with crystals having the composition $U_4O_{8.995}$. Uranium was detected by helium- and deuterium-ion backscattering, and oxygen was detected through protons emitted from the $^{16}O(d,p)^{17}O$ nuclear reaction. Channeling was used to determine that the excess oxygen was not, as had been previously postulated, occupying the centers of the large interstitial holes of the fluorite structure but was instead being incorporated into locations which were removed from both the normal lattice sites and from the interstitial holes by more than 0.2 Å. The channeling data also indicated that, in contrast to a high degree of disorder in the oxygen sublattice, the uranium lattice is only slightly disturbed by the presence of excess oxygen.

3. *High-Energy Forward Scattering* — The backscattering technique is best for thin layers of heavy elements on light element substrates because in such cases the backscattered peak occurs at higher energies than result from backscattering from the substrate. As the mass of a given surface element decreases relative to the substrate elements, the energy of the backscattering peak decreases relative to the substrate spectrum and, when the substrate elements are the heavier, the backscattered peak "sits" on top of a relatively large contribution from the substrate. For single crystal substrates, channeling can reduce the relative substrate contribution and so improve the accuracy and sensitivity with which lighter element measurements can be made. For thick amorphous materials the substrate background cannot be reduced and puts limits therefore on the light element mass and concentration which can be practically detected above the background.

If the target sample can be made sufficiently thin so that the lowest backscattered energy from the substrate is higher than the light element backscattering then, once again, the light element will be clearly resolved. The separation between the gold and chromium peaks in Fig. 3 illustrates this point. The technique is difficult, however, in that very thin samples are required.

Meek and Gibson (51) have shown that the technique can be improved if forward scattering is observed and if the collected particles are scattered forward through the crystal instead of back from it. In these experiments the target was tilted to an angle of 45° with respect to the beam, and 1.8-MeV He^+ or 1.0-MeV protons were observed at 90° with respect to the incident beam direction. For carbon on both surfaces of a 9000-Å-thick silicon wafer they obtained a clear separation between the silicon peak and the carbon scattering peaks. The He^+ scattering also resolved the carbon peaks from the front and back surfaces of the silicon, showing that distribution information about carbon within the film could be obtained. The sensitivity was estimated to be a few monolayers of carbon.

The gases hydrogen and helium are subject to additional limitations. Equation (3) shows that no backscattering at all occurs when the beam particle m_1 is equal to or exceeds in mass the element m_2 being measured. Thus helium particle beams produce no backscattering from hydrogen or helium, and proton beams produce no backscattering from hydrogen. However, forward scattering does occur and has some characteristics which can be put to advantage.

In an interesting experiment performed with protons, Cohen, Fink, and Degnan (49) made use of the fact that when particles of equal mass collide, the angle between the directions of the scattered particle and the recoil particle must be 90°. Thus if an incident proton is deflected through 45° by a hydrogen nucleus (i.e. a proton), the target proton must be emitted at 45° on the other side of the beam. Moreover, in this case, the two protons must have identical energies and, of course, are emitted in time coincidence. The experiments therefore imposed the requirements of 45° deflection, 90° included angle, time coincidence, and equal energy, and provided a measurement which was highly specific to hydrogen and quite sensitive, the sensitivity being estimated to be well below 1 ppm.

Figure 7 is a schematic of the arrangement used. It can be seen from this figure that protons originating from point A, that is at the back surface of the target, arrive at the detectors with greater energy than protons originating from a scattering at point B. There are two reasons for this. One is that the path length through the target is longer from point B, and the second is that because the proton energy after a 45° deflection is only half the original energy, the energy loss per unit path length in the target is increased. The difference in energies corresponding to collisions at points A and B was used therefore to identify the depth at which each event had occurred. For this purpose the pulse heights from the two coincident detectors were summed for each event. The technique is capable of providing not only the amount of hydrogen present in a sample but also its distribution in depth. With a spatial resolution determined by the size of the beam spot, it can also provide information about hydrogen in the plane of the target. The technique furthermore is not limited to extremely thin samples. In the experiments here being cited, 17-MeV protons from a three-stage Van de Graaff accelerator were used to study foils of carbon, Teflon, aluminum, titanium, iron, and zirconium ranging in thickness from 7 mils for the lighter elements to 2 mils for the heavier ones.

Figures 8 and 9, taken from Ref. 49, show some of the results which can be obtained with this technique. Figure 8 is the spectrum (summed coincident pulses) obtained from an Fe-Mylar sandwich target which consisted of three 0.7-mil Fe foils interleaved with four 0.15-mil Mylar sheets. The peaks result from the hydrogen in the Mylar. The difference in peak areas is due mostly to multiple scattering of the protons emerging from the target. The greater the path length a proton must traverse in the target, the more likely the probability that it will undergo scatterings which will cause it to miss the detector; therefore, the peak area becomes progressively smaller the closer a Mylar foil is to the target's front surface. These data show that multiple scattering corrections must be made for thick targets before the true depth distribution can be obtained. Data such as shown in Fig. 8 can be used also to obtain empirical multiple scattering corrections.

Figure 9 shows the hydrogen distribution measured in a 5-mil titanium foil. The dashed lines show the multiple scattering corrections. The two spectra shown correspond to the target being rotated through 180° hydrogen surface contamination on the foil shows up as the two peaks at the ends of the spectrum.

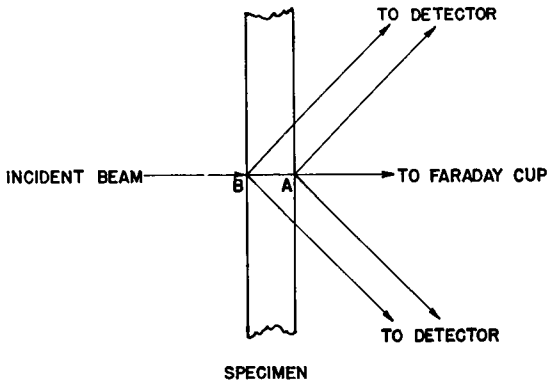

Fig. 7 — Schematic diagram for incident beam, target, and detector geometry used in coincident measurements on scattering between two particles of like mass. (NRL Memorandum Report 2394, Naval Research Laboratory, Washington, D.C., Feb. 1972.)

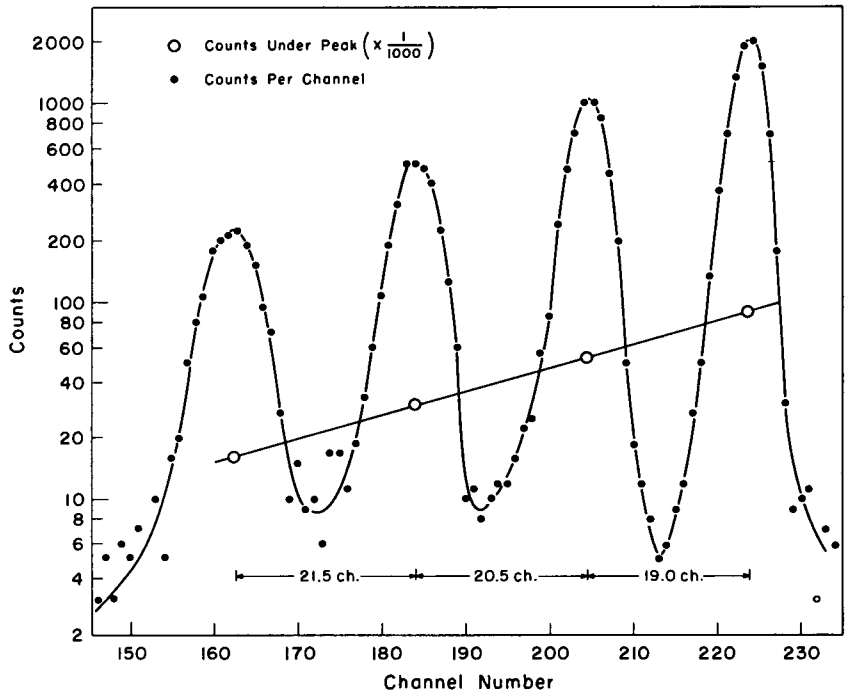

Fig. 8 — Spectrum of summed coincident pulses obtained from hydrogen in a sandwich target consisting of three 0.7-mil Fe foils interleaved with four 0.15-mil Mylar sheets (J. Appl. Phys. 43, 19 (1972))

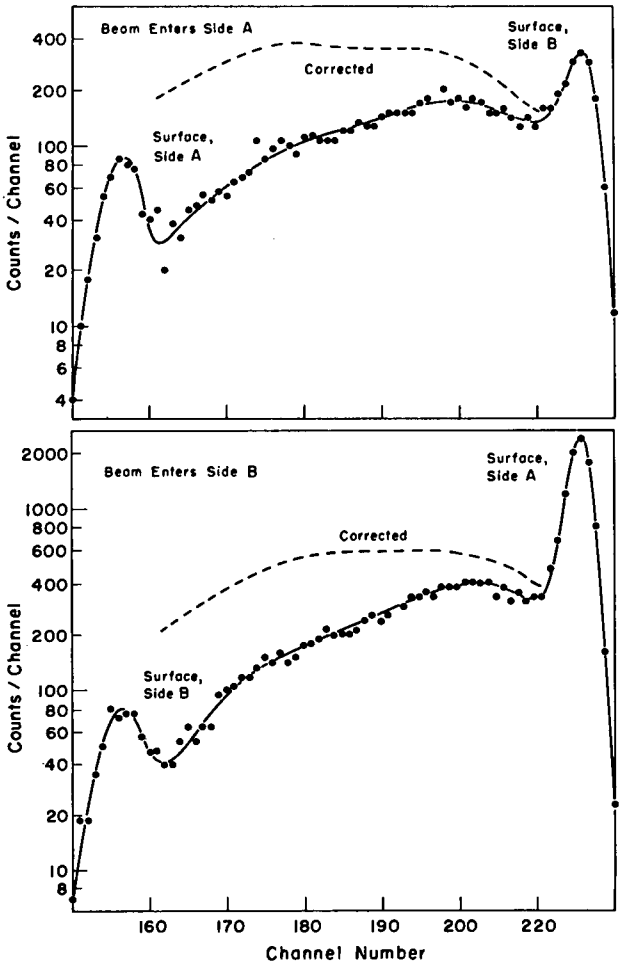

Fig. 9 — Spectrum of summed coincident pulses obtained from hydrogen in a 5-mil titanium foil (J. Appl. Phys. 43, 19 (1972))

The same technique has been applied recently by Pieper and Theus (74) to measure the distribution of helium implanted into aluminum. In this case helium is used as the incident beam, and the reaction considerations are then identical with the case of protons on hydrogen. Figure 10 shows the results obtained with a 48.5-MeV alpha particle beam from a cyclotron, incident on a target which consisted of two 1-mil-thick aluminum foils, into each of which helium had been implanted to a depth of 0.25 mils, separated by 2.5 mils of aluminum. The two helium peaks were easily resolved. The helium concentration of the lower energy peak was 8000 ppm and that of the higher energy peak was 3000 ppm. Again, the peak areas differ somewhat from the corresponding ratio because of multiple scattering effects. Sensitivity is estimated to be 1 ppm or better. Interest in helium in metals in these experiments was associated with the helium embrittlement produced in nuclear reactor materials as a result of (n,α) reactions.

An interesting variation of the elastic scattering technique has been reported by T. A. Cahill (75) in which recoil target nuclei are detected at forward angles, instead of the beam particles. The technique is applicable to the analysis of light elements in thin samples and is quite sensitive. It is being applied to the study of light elements in atmospheric aerosols.

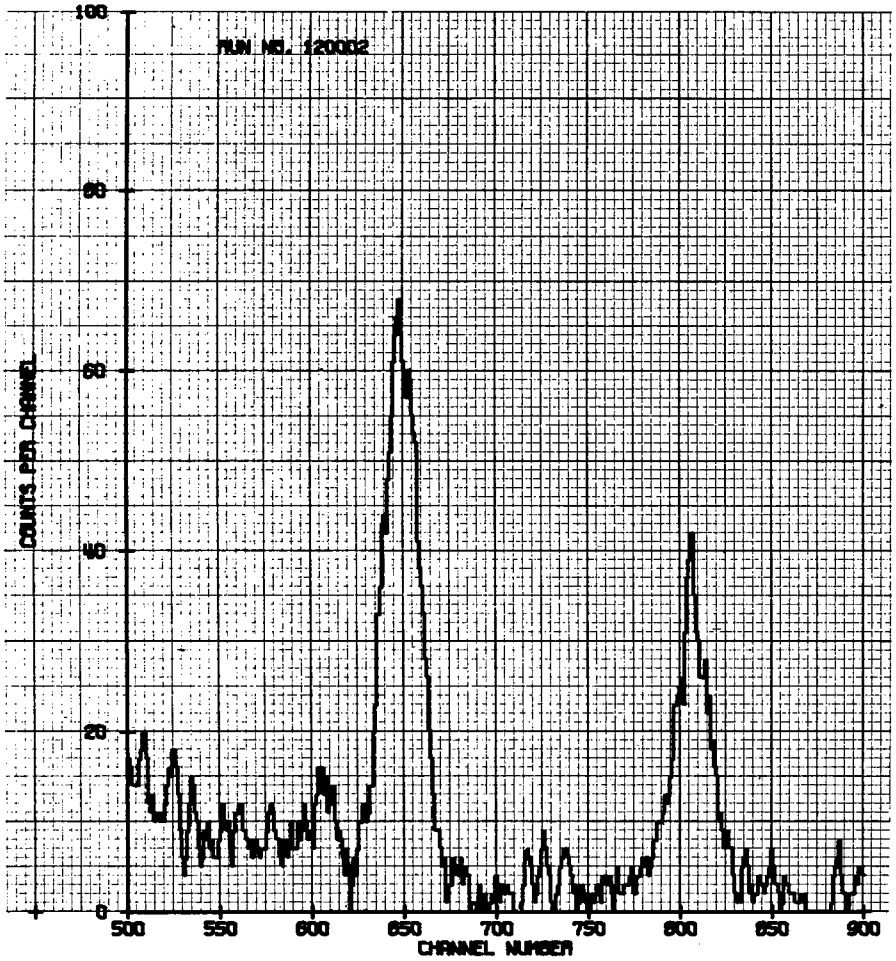

Fig. 10 — Spectrum of pulses obtained from two layers of helium implanted into Al and separated by 2.5 mils of Al (Ref. 74)

4. *Low-Energy Backscattering* — When the incident ion beam energy is between 0.5 and approximately 3.0 keV, the characteristics of backscattering are different in several respects from the high-energy backscattering previously discussed. The importance of the applications made possible by these differences and the low cost of the equipment required as compared to that required for high-energy backscattering and even to that required at 100 keV are such that a separate section devoted to this low-energy range was deemed to be warranted. The region below 500 eV is excluded from the present discussion because it is less well understood and because its utility for surface analyses is still an open question.

The application of low-energy ion scattering to surface analysis was pioneered in a very interesting set of experiments by Smith (38-47). Figure 11 is a schematic of the experimental arrangement used in this work. A compact and relatively simple apparatus was developed by Smith and Goff (76) to facilitate application of the technique in other laboratories. More recently Ball and others (77) have investigated the factors which must be taken into account before measurements can be made quantitative.

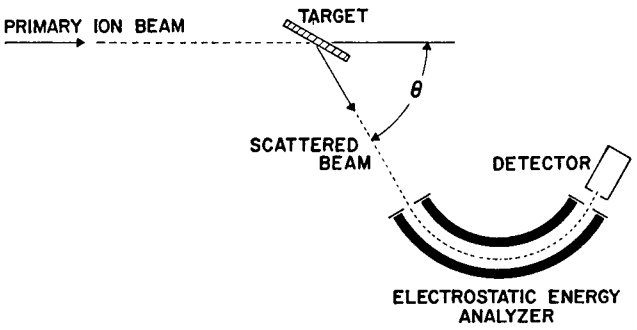

Fig. 11 — Schematic diagram of the arrangement used for low-energy scattering studies of surfaces (Surface Sci. 25, 171 (1971); copyright owned by North-Holland Publishing Company, Netherlands. Used by permission.)

Two major differences exist between backscattering at low energy, $0.5 \leqslant E \leqslant 3.0$ keV, and at high energy, $E > 100$ keV. The first is that the cross section for the low-energy scattering is no longer Rutherford; therefore, it is not given simply by Eq. (5). Instead, cross sections are derived from the screened Coulomb potential (77), a parametrized tabulation for which has been given by Everhart, Stone, and Carbone (78).

The second and more important difference is that at low energies the backscattered particle has a significant probability of having its charge state neutralized. This probability increases as the path length of the particle in the target increases and as the energy of the particle decreases. Thus, for example, particles scattered from beneath the surface are more likely to be neutralized than those which scatter in the topmost atom layers of the target surface. This effect, when combined with an electrostatic analyzer which rejects neutral particles, produces the important consequence that low-energy backscattering analysis can be made sensitive to just the first atom layer of the target surface (47,77). (The neutralization probability also depends on the nature of the incident ion; reactive element ions show less of a tendency for becoming neutralized after scattering from atoms beneath the surface and are therefore less useful for surface analyses (47).)

Figure 12, taken from Ref. 77, illustrates the neutralization characteristic. The figure shows the intensity, on a semilog plot, of alpha particles backscattered from gold through 120° and at various incident energies; for this angle of scattering E/E_0 is expected to be 0.94. Note that at 25 keV there is a plateau and an energy cutoff at $E_1/E_0 = 0.94$. This curve can be compared with the helium—gold backscatter peak in Fig. 3, where the lower energy portion of the peak corresponds to alphas that have been scattered from progressively deeper portions of the gold layer. The target used for Fig. 12 was thick enough so that the intensity of alpha particles should be relatively flat down to the lowest energies. The decreased intensity at lower energies is evidence for the fact that alpha particles coming from beneath the surface are increasingly neutralized and do not get through the electrostatic analyzer to the detector. As the incident beam energy is lowered, this effect becomes more pronounced, until a very sharp peak is observed at 2 keV, even though the gold target is thick to the beam. At this point, clearly, the interfering contributions from the bulk of the target have been effectively eliminated, and the technique can be used to measure surface impurities with high sensitivity.

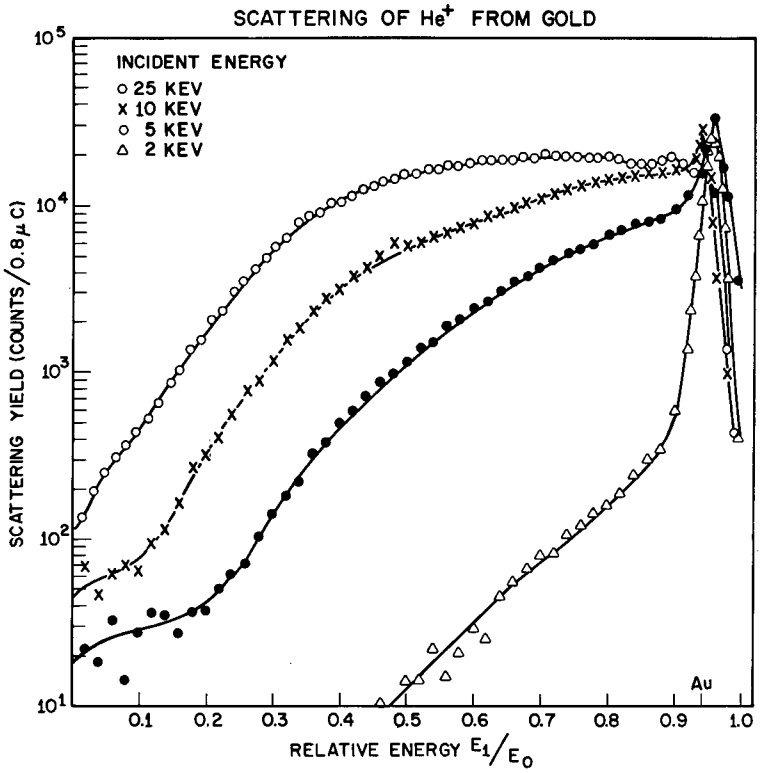

Fig. 12 — Scattering yield of low energy protons as a function of observed energy for various incident energies (Surface Sci. 30, 69 (1972); copyright owned by North-Holland Publishing Company, Netherlands. Used by permission.)

As another illustration, the energy spectrum obtained by Smith (47) in the 90° scattering of 2-keV He^+ ions from polycrystalline copper is shown in Fig. 13 on a linear plot. Again, at higher energies the spectrum would be, not a single sharp peak, but a flat plateau with a sharp cutoff at the peak position.

An interesting result of the technique's sensitivity to just the first layer of surface atoms is shown in Fig. 14, also taken from the work of Smith (47). The figure shows the different spectra obtained when 2-keV He^+ ions are scattered from the two polar surfaces of single crystal CdS. The difference is ascribed to the noncentrosymmetric crystal structure of the compound which has one polar face comprised of Cd atoms and the other comprised of S.

The sensitivity of the low-energy scattering technique to the structure of the top surface layer of atoms was exploited also by Heiland and Taglauer (79) who studied the sorption of oxygen on the ⟨100⟩ face of single crystal nickel. By varying the angle of incidence and the crystal orientation, these authors were able to show that every second place in the ⟨110⟩ row of nickel is occupied by oxygen. From a shadow effect at small angles of incidence they also concluded that the oxygen protrudes from the surface by about 0.5 to 1.0 angstrom units.

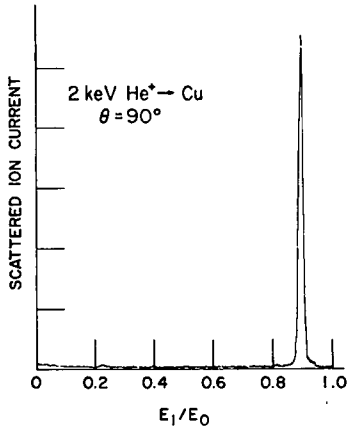

Fig. 13 — Spectrum of 2 keV He^+ ions scattered through 90° from copper (Surface Sci. 25, 171 (1971); copyright owned by North-Holland Publishing Company, Netherlands. Used by permission.)

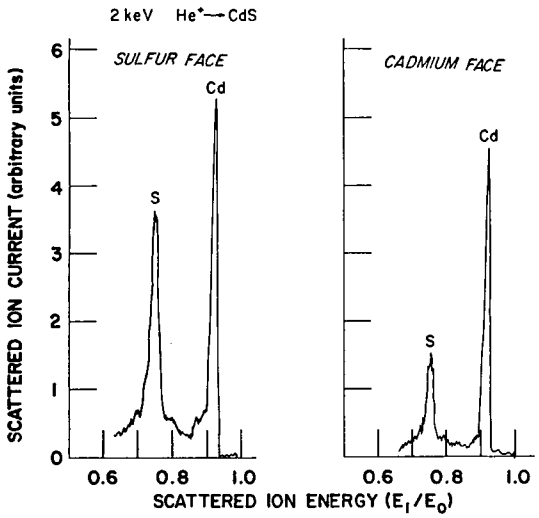

Fig. 14 — Spectra obtained when 2 keV He^+ ions are scattered from the two polar surfaces of single crystal CdS (Surface Sci. 25, 171 (1971); copyright owned by North-Holland Publishing Company, Netherlands. Used by permission.)

Because a single-atom layer of an impurity film on the surface of a sample can completely mask the underlying surface, low-energy scattering measurements must be performed in ultrahigh vacuum, that is at 10^{-9} torr and better, and great care must be taken to remove extraneous surface impurities. For particles heavier than He^+ the sputtering away of the sample by the incident beam must also be taken into account. In addition to these two factors, calibration problems involve evaluation of the charge neutralization probability in collisions with the first layer of atoms, and the dependence of this probability on the elemental composition of the surface.

Low-energy scattering measurements can detect both light and heavy elements on amorphous and crystalline surfaces with sensitivities ranging in some cases down to 10^{-4} atom layers. The technique can be used to study the first surface layer only and is relatively inexpensive. It should therefore come into increasing use for surface studies, along with such techniques as LEED, ESCA, and Auger spectroscopy.

B. Heavy-Ion-Induced X Rays

Considerable interest has developed in the last two years in the use of energetic protons, alpha particles, and other heavy ions for elemental analysis of samples through the characteristic x rays induced by bombardments with these ions. The principal advantage of this technique comes about because heavy ions produce bremsstrahlung background, which is orders of magnitude lower than that produced by electrons. Birks and others (80) compared line-to-background ratios for 15- and 34-keV electrons and 0.7- to 2.0-MeV protons and found the ratios improved by at least one to two orders of magnitude and possibly more. Poole and Shaw (81), recognizing the advantages of proton x-ray excitation, developed a 100-keV, 10-μm-beam-diameter proton microprobe for surface analysis. They achieved a sensitivity of 10 ppm and estimated that 1 ppm could also be achieved.

Recent interest has resulted in part from the advent of high-resolution silicon x-ray detectors which make possible efficient multielement analysis. Johansson and coworkers (82), in an important paper, have given a new impetus to the field by pointing out that the sensitivity of the technique could extend to the 10^{-12}-g level and beyond. For samples which are prepared by the evaporation of droplets of a solution, this number translates into a parts-per-billion sensitivity.

Until recently, the thin beryllium window covering commercially available lithium-drifted-silicon x-ray detectors limited the use of these detectors to elements with $Z \geqslant \sim 12$. Presently, however, detectors are available with windows sufficiently thin so that elements down to oxygen and possibly below can be measured. Specially constructed proportional counters (83) have been used to detect even the ultrasoft K_α radiation from boron. Recent experimentation has occurred at incident-beam energies from 20 keV to 50 MeV and above with incident ion masses ranging from the proton to krypton ions and above (75,80-91).

The large sample loads required in environmental pollution studies and in medical trace element research have spurred the development of highly automatic, computerized systems which can perform multielement analyses on thousands of samples per day. For atmospheric pollution samples, Cahill (75), has, for example, reported analysis costs of between \$1.50 to \$5.00 per sample, for sensitivities of between 10 and 1 ng/cm^3 of air.

The bremsstrahlung radiation produced by heavy ions is caused mainly by the secondary electrons scattered by the passage of the ion through the target material. Highest sensitivity for surface analysis is obtained if the sample is made as thin as possible. Even for thick samples, ppm sensitivities are easily achievable with protons and alpha particles of a few MeV in energy. The number of characteristic x rays produced can again be given by Eq. (1), the reaction yield formula, provided that the cross section $\sigma(E)$ contains both the cross section for ionizing the electron shell in question and the fluorescence yield for the particular x-ray peak being used in the measurement.

Calibration of a measurement is simplest for thin targets since the incident ion energy does not change appreciably in the target and since absorption of the emitted x rays in the target can be neglected. For thick targets, calibration standards and procedures similar to those used for electron microprobe work are required.

The effects of background, counter resolution, type of incident ion, and incident energy on detection sensitivity have been analyzed by a number of authors (84-88). The energy at which a maximum is achieved in the x-ray excitation cross section increases with increasing target atomic number and with increasing beam ion mass. Figure 15 shows K and L x-ray production cross sections calculated for protons by Gordon and Kraner (84). The corresponding maxima for alpha particles occur at higher energies than for protons. At Van de Graaff accelerator facilities, typically, protons are used for x-ray analysis; at cyclotrons alpha particles are used.

An interesting application to x-ray analysis of the heavy ions K, V, and Kr with energies in the range from 20 to 220 keV has been made by Cairns and coworkers (90). These authors show that it is possible in certain cases to excite characteristic x rays in a selective manner by adjusting the bombarding energy. Thus, for example, when a potassium beam is incident on copper, the threshold for copper L-x-ray production occurs at 40 keV while the threshold for potassium L-x-rays occurs at approximately 20 keV; it is therefore possible below 40 keV to excite the latter x-rays preferentially. This technique, which is particularly sensitive to elements at or near the surface, has been applied (91) in conjunction with anodic stripping to the determination of depth distributions of antimony implanted into silicon.

An example of the kind of spectrum that can easily be achieved with heavy-ion-induced x rays and lithium-drifted silicon detectors is shown in Fig. 16. These data were obtained by Knudson and Wilkniss (92) from the irradiation of a thin layer of sediment which had been collected from a municipal water reservoir. The sample in this run, consisting of approximately 30 $\mu g/cm^2$ of material deposited in a thin, self-supporting Zapon lacquer film, was bombarded for approximately 7.5 min with a 44-NA beam of 5.0 MeV protons. The lower energy cutoff in the spectrum is due to two beryllium windows, with a total thickness of 9 mils, present between the target and the detector.

At the present stage of development, heavy-ion-induced x-ray analysis is best suited to multielement measurements in thin samples. The recent availability of ultrathin window lithium-drifted silicon detectors should promote research investigations on the gaseous elements nitrogen, oxygen, and fluorine. Another interesting possibility for the future is the recent discovery that chemical bonding can affect heavy ion induced K-x-ray spectra (93).

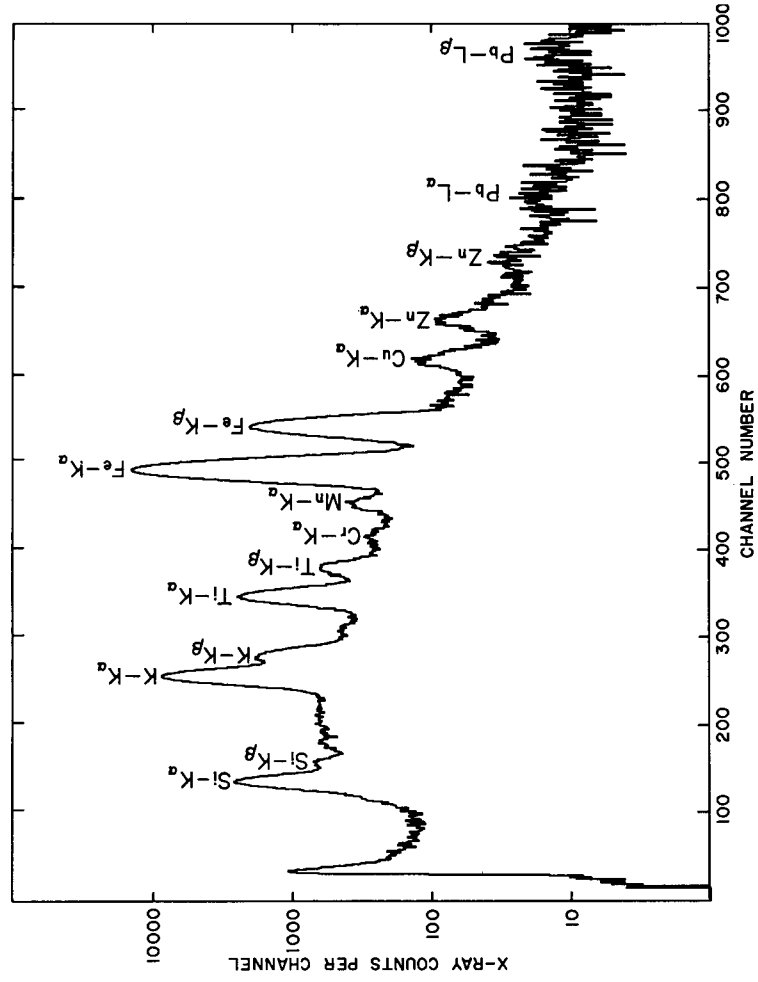

Fig. 16 — Yield of x rays obtained from the irradiation of sediment from a municipal water reservoir with 5.0 MeV protons (Ref. 92)

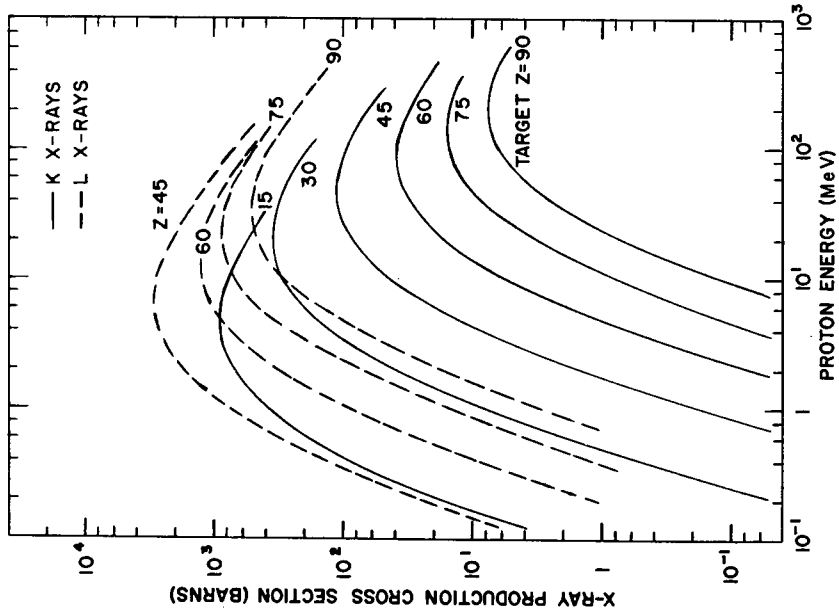

Fig. 15 — Calculated cross sections for x-ray production by protons

C. Nuclear Reactions

When the incident beam particle has enough energy to penetrate through the electrostatic Coulomb repulsion which develops as it approaches the nucleus of a target atom, a nuclear reaction can occur. Symbolically a nuclear reaction maybe written

$$a + T \rightarrow b + R + Q, \tag{11}$$

where

a = incident nucleus
T = target nucleus
b = emitted radiation
R = residual nucleus
Q = energy released (absorbed) in the reaction.

Nuclear reactions can be exoergic, in which case Q is positive; or endoergic, in which case Q is negative. If the residual nucleus R is left in an excited state the Q for the reaction is reduced relative to the value which would obtain if the residual nucleus were left in its ground state by the amount of the excitation energy. The emitted radiation b can be a nuclear particle or one or more gamma rays. The case a = b and Q = O is simply the elastic scattering reaction which has been discussed previously. Inelastic scattering corresponds then to a = b and $Q < O$. When $a \neq b$ the reaction is termed a rearrangement collision.

The conservation of total energy and momentum lead to the following expression (nonrelativistic) for the energy E_b of a nuclear particle which is emitted from a reaction:

$$E_b = E_a \frac{M_a M_b}{(M_b + M_R)^2} \left\{ 2\cos^2\theta + \frac{M_R(M_b + M_R)}{M_a M_b} \left[\frac{Q}{E_a} + \left(1 - \frac{M_a}{M_R} \right) \right] \right.$$
$$\left. \pm 2\cos\theta \left[\cos^2\theta + \frac{M_R(M_b + M_R)}{M_a M_b} \left\{ \frac{Q}{E_a} + \left(1 - \frac{M_a}{M_R} \right) \right] \right]^{1/2} \right\}. \tag{12}$$

E and M are energy and mass, respectively, and the subscript identifies the corresponding particle. In this formula θ is the angle between the emitted particle and the incident beam direction in the laboratory frame of reference. For elastic scattering, Eq. (12) reduces to the Eq. (3) given earlier.

Equation (12) shows that for a given reaction, incident energy E_a, and observation angle θ, the energy spectrum E_b will depend on the Q values possible to the reaction. In a manner quite analogous to optical spectroscopy, if the residual nucleus can be left in any of several sharply defined energy states and if the target is thin so the incident energy has a single well-defined value, the energy spectrum of the emitted particles will exhibit a series of narrow peaks, each of which corresponds to one of the excited states of the residual nucleus. Such a spectrum will then be highly specific to the reaction which has occurred and can be used to identify the presence of a given elemental isotope. The positions of the peaks in the energy spectrum are easily calculable from Eq. (12). The intensity ratios of the various peaks in the spectrum are also characteristic of the reaction and provide additional useful information for identifying the reaction responsible.

In the case of thin targets, the amount of an isotope present can be calculated from the observed reaction yield $Y_b(\theta)$ using the equation

$$Y_b(\theta) = n\ N\ \Delta\ x\ \sigma\ (E,\theta)\ \Omega, \tag{13}$$

where

n = total number of incident beam particles,
N = number of reactant atoms per cubic centimeter,
Δx = target thickness in centimeters,
$\sigma(E,\theta)$ = differential cross section in square centimeters per steradian at energy E and at angle θ,
Ω = solid angle subtended by the detector. This equation is of the same form as Eq. (4), and, when integrated over all angles, as Eq. (1).

For thick targets, the energy dependence of the cross section and any dependence of the concentration on depth in the sample must be taken into account. The thick target formula is then simply

$$Y_b(\theta) = n\Omega \int_0^{\mathcal{R}} N(x)\ \sigma(x,\theta)\ dx, \tag{14}$$

where $\mathcal{R}$ is the range (maximum penetration distance of the incident beam particle in the target, and the relationship between beam energy and depth x in the target is given by

$$E(x) = E_0 - \int_0^x \frac{dE}{dx'}(x')\ dx'. \tag{15}$$

In this equation, E_0 is the beam energy just before it enters the target, and

$$\frac{dE}{dx}(x')$$

is the energy loss of the beam per centimeter of target matter at depth x′; a number of stopping power tables exist which can be used to obtain this quantity. (See, for example, Ref. 27.) Because penetration depth and beam energy are uniquely related, integration over target thickness can be performed either over distance or energy; Eqs. (2) and (14) are therefore basically equivalent.

The problems of target thickness, which were discussed in connection with charged particle activation analysis and Eq. (2), apply also here. Most often, quantitative measurements are obtained by comparison with standard samples. If calculations are used, they are frequently based on approximations which avoid the full-scale integration called for in Eq. (14).

In principle, it should be possible through a series of yield measurements at various incident energies to unfold the depth dependence of N(x). In practice this is difficult to do when the reaction cross section varies only slowly with energy. The special and important case of reactions which exhibit a strong dependence on energy, the so-called resonance reactions, will be discussed for such application in a following section. For nonresonant reactions, information on depth distribution may be obtained in some cases, as is done in the backscattering technique, through careful measurement of the energy losses suffered by the observed particles b.

An experiment performed by Wolicki and Knudson (94) illustrates in a simple way how a nuclear reaction can be applied to surface analysis. In this work it was desired to detect sulfur nondestructively in thin films on a copper-nickel alloy in the presence of carbon and oxygen. The $^{32}S(d,p)^{33}S$ reaction was selected for the measurement because the Q value (6.41 MeV) for this reaction is considerably higher than that for the (d,p) reaction on either carbon or oxygen. Interference from (d,p) reactions on copper and nickel was expected, but the possibility was that it would be small.

Initially a 4.0-MeV deuteron beam was used to bombard the samples. At this energy, the intensity of protons from reactions produced in the copper and nickel isotopes was so high that the protons due to the thin sulfur film could not be observed. The deuteron beam energy was then reduced to 2.0 MeV. Because of the different Coulomb barriers involved, this reduction in beam energy produced a very large preferential reduction of the (d,p) yields from copper (Z = 29) and nickel (Z = 28) relative to those from sulfur (Z = 16). The discrete spectrum due to the thin sulfur film was thereby rendered easily identifiable.

The spectrum of protons obtained with a test sulfide film is shown in Fig. 17. The arrows labeled with symbols p_0 through p_8 show the energies calculated from Eq. (12) for protons emitted from the $^{32}S(d,p)^{33}S$ reaction. The symbol p_0 labels protons which correspond to ^{33}S being left in its ground state; p_1 corresponds to the first excited state of ^{33}S, and so on. The correspondence of so many peaks with the expected energies provides a positive identification of sulfur on the irradiated sample. Not only the energy positions of the peaks, but also the relative heights and, for some reactions, the widths of the peaks are all characteristic of the reaction responsible for the emitted particles. The sensitivity of the measurement was estimated to be easily 10^{-7} g/cm^2, with the possibility for considerable improvement beyond this value.

An excellent article on the analysis of oxygen by nuclear reactions has been written by Amsel and Samuel (95). These authors discuss the reactions $^{18}O(p,\alpha)^{15}N$, $^{18}O(d,\alpha)^{16}N$, $^{16}O(d,\alpha)^{14}N$, $^{18}O(d,p)^{19}O$, and $^{16}O(d,p)^{17}O$. In each case the reaction is observed through the emitted charged particles. Relatively low bombarding energies (up to 600 keV) can be used, and the measurements determine either the absolute amount of each isotope of oxygen or the ratio $^{18}O/^{16}O$. The reactions are highly specific, and amounts of the order of 10^{-12} gram of ^{18}O can be detected. The article also discusses the advantages of these measurements over all others, including nonnuclear analyses, and gives methods for correcting for targets of finite thickness.

The use of a 2-MeV Van de Graaff accelerator for the nuclear reaction analysis for carbon, nitrogen, oxygen, fluorine and other elements has been discussed by Amsel and others (96). The article includes a list of the most useful reactions along with discussions of the principles involved, particle detection instrumentation, concentration profile measurements with both resonant and nonresonant nuclear reactions, and several interesting applications.

Barrandon and others (97) have studied (d,p) reactions for determining carbon and oxygen in the surfaces of metal samples. Results from the prompt radiation analysis were compared with charged particle activation analysis through the $^{12}C(d,n)^{13}N$ and $^{16}O(t,n)^{18}F$ reactions and were found to be in agreement. Through these analyses it was discovered and quantitatively demonstrated that, whatever the metal, the sample surface always contains a certain quantity of carbon and oxygen after cleaning. It was also shown

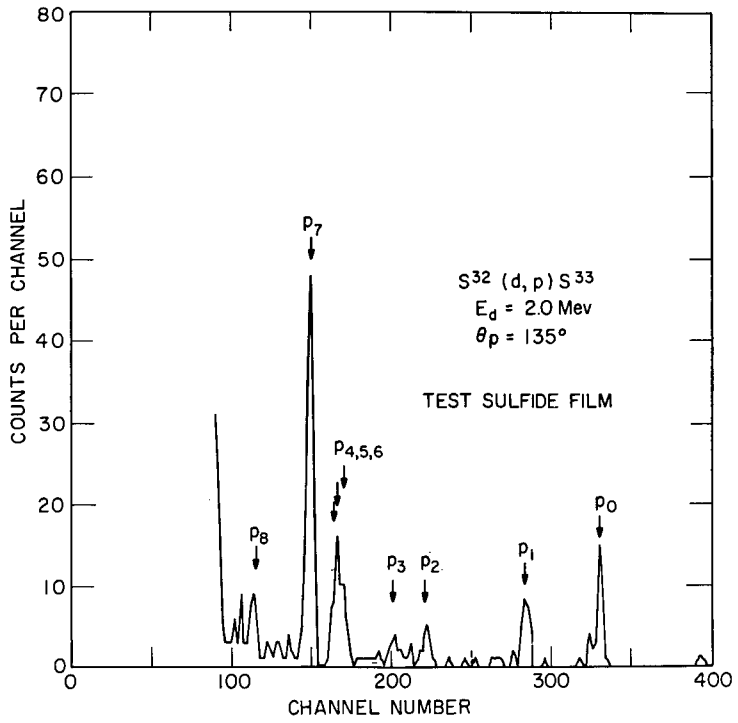

Fig. 17 — Spectrum of protons emitted from the $^{32}S(d,p)^{33}S$ reaction in a 2.0-MeV deuteron irradiation of a thin Sulfide film on a nickel alloy (Int. J. Appl. Radiat. Isotop. 18, 429 (1967); copyrighted by Pergamon Press, Ltd. Used by permission.)

that this surface contamination causes an error in bulk carbon and oxygen determinations by fusion reduction and combustion and in oxygen determinations by 14-MeV neutron bombardment. On the other hand, with charged particle activation analysis, since the ^{13}N and ^{18}F radioactivities used are relatively long, it is possible to eliminate this error by cleaning the samples after radioactivation but before radiation measurements.

Oxygen diffusion in quartz has been studied by Palmer (98) through the use of enriched ^{18}O and the $^{18}O(p,\alpha)^{15}N$ reaction. Information on the concentration profile of the ^{18}O was obtained through measurements on the energies of the observed alpha particles. The experimental α-particle energy resolution was 100 keV and corresponded to a depth resolution of approximately 2500 Å.

Prompt neutron radiation from nuclear reactions has been used for analysis by Möller and coworkers (99) and by Peisach (100). Reference 99 discusses the use of (d,n) reactions to determine impurities of carbon, nitrogen, and oxygen on and below steel surfaces. Samples were irradiated by 3-MeV deuterons and the spectra of emitted neutrons were measured by the time-of-flight method. Sensitivity was estimated to be 0.1 $\mu g/cm^2$ and the depth resolution, obtained from the shape of the peaks in the neutron spectra, was estimated to be 4500 Å.

Although the preceding discussion has dealt exclusively with emitted nuclear particles and Eq. (12) is derived for this case, prompt gamma radiation from nuclear reactions can also be used for analysis. The energy spectrum of the gamma rays is then characteristic of the nuclear reaction produced. A reaction mode, called direct capture, for which the emitted gamma ray energy depends on the incident beam energy, is also possible. By combining the excellent resolution of Ge(Li) detectors with this mode in the $^{16}O(p,\gamma)^{17}F$ reaction, Joy and Barnes (101) were able recently to achieve depth distribution measurements on oxygen in metals.

D. Nuclear Resonance Reactions

Many nuclear reactions have the property that the reaction yield exhibits resonances at one or more sharply defined incident ion energies. Experimentally such a yield curve is obtained, one point at a time, by a variation of the incident beam energy in small increments and a measurement of the quantity of emitted radiation per unit incident beam fluence (number of particles incident on a unit cross-sectional area) at each energy. The resonances and their energy widths correspond to the energy levels and level widths, respectively, in the compound nucleus which is formed. With reference to Eq. (11), the compound nucleus formed is (a + T); the emitted radiation b can again be one or more gamma rays or a nuclear particle. In somewhat simplified form, the resonant reaction cross section can be written

$$\sigma(E) = \frac{\sigma_0}{(E - E_R)^2 + \frac{\Gamma^2}{4}}, \tag{16}$$

where E_R is the resonance energy, Γ is the full width of the resonance at half maximum, and σ_0 is the peak cross section at resonance.

From the standpoint of elemental analysis, the resonance properties of a nuclear reaction are of interest for two reasons. The first is that the resonance energy E_R is characteristic of a particular nuclear reaction and can be used for identifying that reaction and for making a selective measurement on one element (actually just one isotope of that element) in the presence of many others. The second is that the energy dependence of the cross section, when combined with the energy loss of the incident beam as it penetrates into the target, makes possible depth distribution measurements on the element in question. Of particular importance is the fact that nuclear reaction resonances can be sufficiently sharp so that depth resolutions better than 100 Å can, in some cases, be achieved. For such high resolution, the resonance width and the energy loss of the beam in the target must be accurately taken into account.

The width Γ of the reaction yield curve which is observed experimentally is composed of three parts: the intrinsic width of the level in which the compound nucleus is formed, doppler broadening due to the thermal motion of the reactant target atoms, and the energy inhomogeneity of the incident beam particles. The intrinsic width of a resonance depends only on the characteristics of the corresponding compound nucleus energy level, so it needs to be evaluated only once for a particular resonance. The doppler broadening can be calculated to a useful accuracy from the Debye temperature of a material. The energy inhomogeneity of the beam depends not only on the way in which the beam is prepared but also on the variations in energy loss which occur because of the statistical

nature of the energy loss process as a charged particle traverses matter. Because of this energy loss straggling, as it is called, the energy inhomogeneity is a function of the depth of the beam as it penetrates into the target. When all the above factors are known, an experimentally observed yield curve Y(E) can be unfolded to give the depth distribution N(x) of the reactant atoms, provided the beam energy inhomogeneity is not overly large. The calculation, which involves a triple integration, requires the use of a large digital computer program (102).

A recent set of measurements on the depth distribution of a thin layer of aluminum within a silicon dioxide surface (103) provides a simple example for illustrating how the nuclear reaction resonance technique is used in practice and what kinds of results can be achieved with it. This case is a good example for discussion because the $^{27}Al(p,\gamma)^{28}Si$ reaction, the reaction used for these measurements has an unusually sharp resonance and a relatively large peak cross section. The depth resolution and quantitative sensitivity of the technique are therefore both good.

Consider a target sample as shown in the top portion of Fig. 18. The sample consists of SiO_2 containing two thin layers of Al, one at the very surface and another, with a lower density of Al atoms in it, at some distance in from the surface.

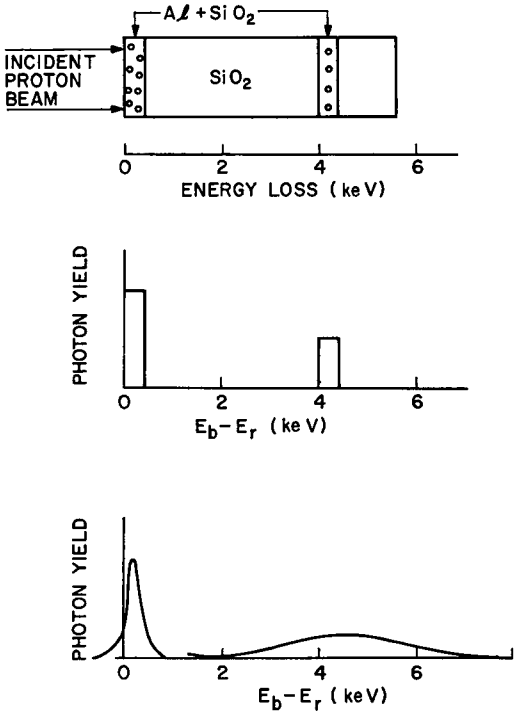

Fig. 18 — Schematic diagrams showing a SiO_2 sample containing two thin layers of Al, and the corresponding idealized and real yield curves for the $^{27}Al(p,\gamma)^{28}Si$ reaction (Ref. 103)

For the ideal case of an infinitely narrow resonance width, a perfectly monoenergetic proton beam, and no straggling in energy loss as the beam penetrates into the target, the gamma-ray yield curves which would be obtained are shown in the middle portion of the figure. Along the abscissa is plotted the difference between the incident beam energy and the reaction resonance energy. For the surface layer the yield starts at the resonance energy, and the width of the yield curve in energy units is proportional to the thickness in atoms per square centimeter of the Al-SiO_2 layer. The width of the curve is, of course, due to the energy loss the protons undergo as they traverse the Al-SiO_2 layer. Thus while the SiO_2 does not contribute to the gamma-ray yield, it does cause the protons to lose energy and so must be taken into account along with the Al where the width of the yield curve is concerned. The area under the curve is proportional to the number of Al atoms per square centimeter in the layer.

For the internal layer as it is shown, the resonance is displaced to a higher proton energy by 4 keV because the protons have lost this amount of energy in traversing the material between the surface and the internal layer. Since the density of Al atoms is somewhat lower in this layer than in the surface layer, the yield is correspondingly lower. The width of the yield curve is again proportional to the thickness of the Al-SiO_2 layer, and the area is proportional to the amount of Al.

The real situation is shown in the bottom part of the figure. The yield curves shown now reflect the real width of the resonance, doppler broadening due to the thermal motion of the Al atoms, inhomogeneity in the beam energy, and beam energy loss straggling. It is this last factor that so greatly broadens the yield curve obtained for the internal layer. Given the distribution of the Al in the SiO_2 as shown in the top of the figure, the intrinsic width of the resonance, the beam energy inhomogeneity, and the computer program of reference (102), it is possible to predict the yield curves shown at the bottom of the figure. Conversely if a yield curve is observed as shown, the program can, by iteration, be used to obtain the Al distribution.

Results obtained by Dunning (103) for a SiO_2 sample into which 60-keV Al atoms were implanted to a fluence of 1×10^{15} atoms/cm^2 are shown in Fig. 19. The open triangles are the theoretical fit to the data and the crosses are the Al depth distribution required to fit the data. The measurements showed that while the bulk of the Al had the depth distribution expected for a 60-keV implantation, there was a small concentration of Al very close to the surface. The reasons why some of the Al came to rest at that depth are not known. The number of iterations required to obtain the depth distribution was four, a relatively small number. The depth resolution obtained in the measurements was estimated to be between 50 and 100 Å. For this work the resonance in the $^{27}Al(p,\gamma)^{28}$ Si reaction which occurs at 992 keV was used. This resonance has an intrinsic width of approximately 100 eV (104). With a magnetic or electrostatic beam energy analysis system and a suitably thin Al target, an experimental yield curve width of 1 keV or less is readily achievable for this reaction. The depth resolution of 50 to 100 Å comes about because the center of the resonance can be determined with a relative accuracy which is better than the full width of the resonance.

Results from a somewhat different application of the same resonance reaction are shown in Fig. 20. In these experiments, performed by Bernett and others (105), the object was to measure the amount of aluminum oxide power, grit size 0.3 μm in diameter, which remained in metals of various hardnesses after these metals had been polished with this powder and then rinsed clean.

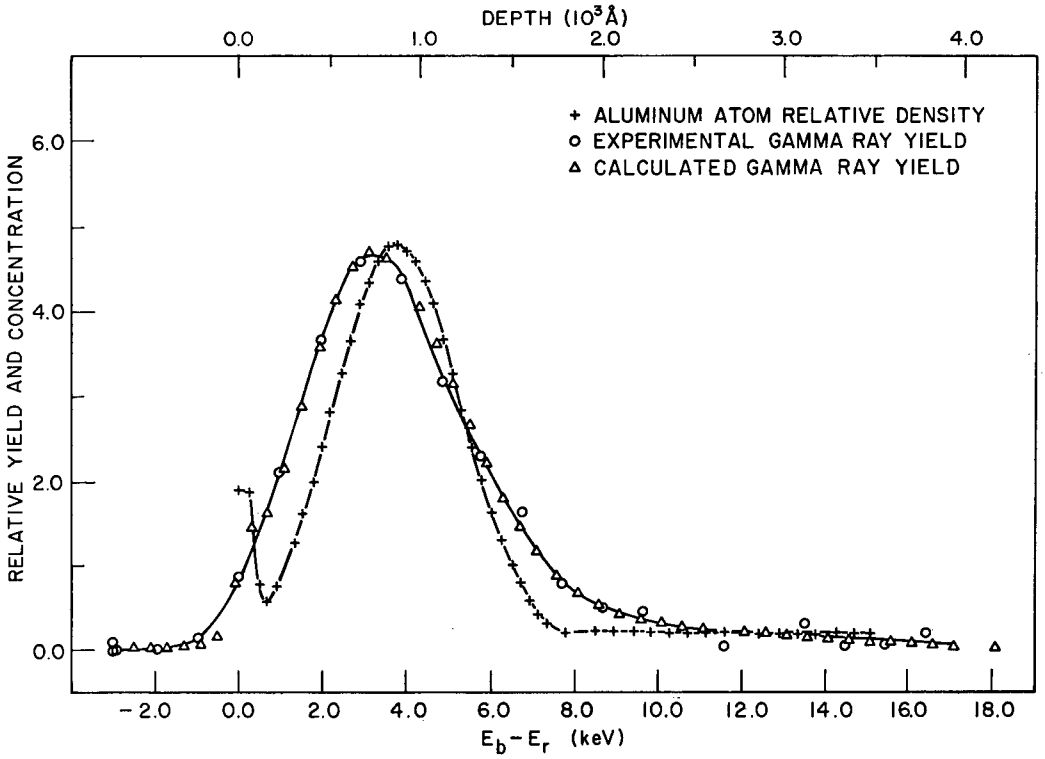

Fig. 19 — Experimental and calculated gamma ray yield curves and a depth distribution profile obtained for a thin layer of Al implanted into SiO_2 (Ref. 103)

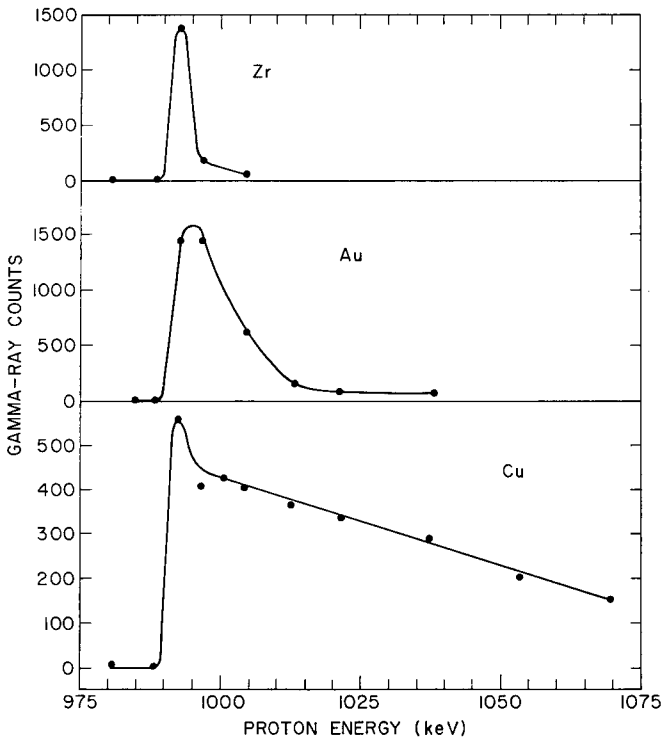

Fig. 20 — Yield curves for the $^{27}Al(p,\gamma)$ ^{28}Si reaction for Al_2O_3 polishing compound retained in Zr, Au, and Cu surfaces (J. Appl. Phys. 42, 5826 (1971))

The top figure shows the results obtained for zirconium. The resonance was observed at the correct energy for the grit particles to be located right on the surface of the sample, and the width of the yield curve corresponds closely to the 0.3-μm diameter of these particles. The area under the curve is proportional to the average number of Al atoms per square centimeter.

The middle figure shows the results of a similar measurement for gold. This curve has a greater area and is broader than the first; these features show, respectively, that more polishing compound has been retained in the sample and that some of the particles are embedded in the gold. Finally, the bottom curve shows that in copper there is still more polishing compound retained in the sample and that the grit particles are embedded still more deeply. In the latter case the interesting finding was that some of the particles are buried at least 1 μm deep and are covered over by the copper, even though the polishing was performed by hand on a relatively slow-moving polishing surface. The thickness of copper covering the Al_2O_3 particles is evidenced by the fact that the reaction yield is still appreciable at 1080 keV, an energy which is over 90 keV above the resonance energy.

Measurements of fluorine contamination on and below the surface of Zircaloy were performed by Möller and Starfelt (106) by means of a resonance at 1375 keV in the $^{19}F(p,\alpha\gamma)^{16}O$ reaction. The notation in this case means that the compound nucleus ^{20}Ne, formed by the proton's capture in ^{19}F, decays by α emission to an excited energy state of ^{16}O which then emits gamma rays as it decays to its ground state. The α and γ emissions, although sequential, occur in such extremely short times that for all practical purposes they can be considered as instantaneous. The fluorine present in a sample can be observed through the gamma rays, and for thin samples, also through the alpha particles; in the present case the gamma rays were used and both the total amount and the depth distribution of the fluorine were measured for a number of Zircaloy samples which had undergone different treatments. Although 29 samples were studied. The samples had been ground, pickled, or electropolished, and had undergone autoclave treatments varying in temperature and time. It was found that the unoxidized samples contain fluorine only on the surface or in a surface layer thinner than 0.1 μm. In the oxidized samples, the fluorine was found to be distributed down to depths of several microns. The yield from this reaction is sufficiently high so that a quantity of fluorine less than 0.01 $\mu g/cm^2$ can be detected by this method.

Chemin and others (107) have used resonances in $(p,p'\gamma)$ nuclear reactions to measure trace amounts of Si and S in GaSb. The notation $(p,p'\gamma)$ means that after the compound nucleus is formed by proton capture in the target nucleus, the proton is reemitted with a reduced energy, leaving the target nucleus in an excited energy state which then decays to the ground state by the emission of one or more gamma rays.

The specific reactions used in these studies were the $^{28}Si(p,p'\gamma)^{28}Si$ and the $^{32}S(p,p'\gamma)^{32}S$. For the silicon reaction, resonances at 3100 and 3335 keV were used; for the sulfur reaction the principal resonance used was that at 3379 keV. These reactions provided the excellent detection sensitivities of 0.12×10^{-9} g for sulfur and 0.16×10^{-9} g for silicon. Comparison was made with detection sensitivities for spectrophotometry, fluorescence, atomic absorption, flame spectrophotometry, neutron activation analysis, and spark source mass spectroscopy. Only spark source mass spectroscopy, with a sensitivity of 0.03×10^{-9} g for both silicon and sulfur, exceeded the sensitivity of the $(p,p'\gamma)$ resonance reaction technique. In general, the remaining techniques were two to four orders of magnitude less sensitive than the resonance technique.

As a final example, Whitton and coworkers (108) used the 639-keV resonance in the $^{18}O(p,\alpha)^{15}N$ reaction to measure the depth distribution of oxygen implanted into gallium phosphide at implantation energies of 20, 40, and 60 keV. These experiments differ from the previous examples cited in that the emitted radiation observed consisted not of gamma rays but of alpha particles. The quantity of ^{18}O implanted in various samples varied from approximately 2×10^{15} atoms/cm^2 to 7×10^{15} atoms/cm^2; these values correspond, respectively, to 6×10^{-8} and 21×10^{-8} g/cm^2 of ^{18}O. Depth distribution curves for the implanted ^{18}O were measured before and after annealing for 15 min in vacuo at 600°C. The shift and broadening of the depth distribution after annealing were found to be consistent with thermal diffusion. The measurements showed that the $^{18}O(p,\alpha)^{15}N$ resonance reaction can be used to distinguish differences in the range and range straggling of oxygen implanted into GaP to depths that are of interest in the formation of electroluminescent devices. The reaction was judged to be useful also for oxygen profiling in a large number of host materials.

ACKNOWLEDGMENT

The author is indebted to Mr. Dean Walter, Head of the Analytical Chemistry Branch, for first suggesting that an article on the applications of ion beams to surface analyses might be of interest to the editors of a book, then in preparation, on the *Determination of Gases In Metals* and for interesting one of the editors, Dr. L. Melnick, in such an article. This suggestion and interest provided the motivation for the preparation of this article. Thanks are due to the publishers, John Wiley and Sons, Inc., for kindly agreeing to separate publication of this material and to T. Buck, B. Cohen, B. Gordon, A. Pieper, and D. Smith for permission to use their previously published figures. The author is grateful also to Drs. J.W. Butler, K.L. Dunning, J.K. Hirvonen, and J.E. Westmoreland for helpful discussions and comments. Further, it is a pleasure to acknowledge the interest and support of Dr. John McElhinney for nuclear and ion beam applications in general and for the preparation of this report in particular.

REFERENCES

1. J.P. Guinn, ed., Proceedings of the 1965 International Conference on *Modern Trends in Activation Analysis* College Station, Texas, Apr. 19-22, 1965, Texas A&M U., College Station, Texas, 1965.

2. *Proceedings of the First Conference on Practical Aspects of Activation Analysis with Charged Particles*, Grenoble, France, June 23, 1965, Euratom, EUR 2957 d-f-e.

3. R.S. Tilbury, "*Activation Analysis with Charged Particles*," Nat. Acad. Sci., Nat. Res. Council Nuclear Science Series, NAS-NS 3110, Clearinghouse for Federal Scientific and Technical Information, Springfield, Va., 1966.

4. A.A. Smales, "Radioactivity Techniques in Trace Characterisation," in *Trace Characterization, Chemical and Physical* (W.W. Meinke and B.F. Scribner, eds.), NBS Monograph 100, Government Printing Office, Washington, D.C., 1967, p. 307.

5. V.P. Guinn, "Nuclear Methods," in *Trace Characterization, Chemical and Physical* (W. W. Meinke and B.F. Scribner, eds.), NBS Monograph 100, Government Printing Office, Washington, D.C., p. 337.

6. *Proceedings of the 2nd Conference on Practical Aspects of Activation Analysis with Charged Particles* (H.G. Ebert, ed.), Liege, Belgium, Sept. 21-22, 1967, Euratom, EUR 3896 d-f-e.

7. *Modern Trends in Activation Analysis*, (J.R. DeVoe, ed.) NBS Special Publication 312, Vols. 1 and 2, Government Printing Office, Washington, D.C., 1969.

8. E.H. Krause, "Particle Accelerators," Section 8 in *American Institute of Physics Handbook*, McGraw-Hill, New York, 1957, Tables 8i-1 and 8i-2.

9. R.H. Marsh and W. Allie, Jr., "High Precision Activation Analysis of Sodium Using an Internal Standard Technique," *Modern Trends in Activation Analysis* (J.R. DeVoe, ed.), NBS Special Publication 312, Vol. II, Government Printing Office, Washington, D.C., 1969, p. 1285.

10. F.F. Dyer, L.C. Bate, and J.E. Strain, "Three-Dimensionally Rotating Sample Holder for 14-Million Electron Volt Neutron Irradiations," Anal. Chem. **39**, 1907 (1967).

11. J. Comas and E.A. Wolicki, "Argon Content in (111) Silicon for Sputtering Energies Below 200 eV," J. Electrochem. Soc. **117**, 1197 (1970).

12. S.S. Markowitz and J.D. Mahony, "Activation Analysis for Oxygen and Other Elements by He^3-Induced Nuclear Reactions," Anal. Chem. **34**, 329 (1962).

13. J.D. Mahony, "Reactions of He^3 with Light Elements: Applications to Activation Analysis," Lawrence Radiation Laboratory Report UCRL 11780 (1965).

14. E.L. Steele, "Helium-3 Charged Particles in Activation Analysis," General Atomic Report GA-6568, San Diego, Calif., 1965.

15. E. Ricci and R.L. Hahn, "Theory and Experiment in Rapid, Sensitive Helium-3 Activation Analysis," Anal. Chem. **37**, 742 (1965).

16. E. Ricci and R.L. Hahn, "Sensitivities for Activation Analysis of 15 Light Elements with 18-MeV Helium-3 Particles," Anal. Chem. **39**, 794 (1967).

17. R.W. Benjamin, L.D. England, K.R. Blake, I.L. Morgan, and C.D. Houston, "Deuteron Activation Analysis for C, N, and O in High-Purity Metallic Surfaces," Trans. Amer. Nucl. Soc. **9**, 104 (1966).

18. J.L. Debrun, J.N. Barrandon, and Ph. Albert, "Contribution to Activation Analysis by Charged Particles; Determination of Carbon and Oxygen in Pure Metals, Possibilities of Sulphur Determination," in *Modern Trends in Activation Analysis* (J.R. DeVoe, ed.) NBS Special Publication 312, Vol. II, Government Printing Office, Washington, D.C., 1969, p. 774.

19. J.N. Barrandon and Ph. Albert, "Determination of Oxygen Present at the Surface of Metals by Irradiation with 2 MeV Tritons," in *Modern Trends in Activation Analysis* (J.R. DeVoe, ed.), NBS Special Publication 312, Vol. II, Government Printing Office, Washington, D.C., 1969, p. 794.

20. G. Revel and Ph. Albert, "A Study of the Possibilities of Measuring Oxygen in Zirconium, Molybdenum, Hafnium and Tungsten by Irradiation with ^3He and ^4He Particles," in *Practical Aspects of Activation Analysis with Charged Particles* (H.G. Ebert, ed.), EUR 3896 d-f-e (1968).

21. P. Albert, "Nuclear Methods for Determination of Oxygen and Carbon on Metal Surfaces," Vide **24**, 149 (1969).

22. J.W. Butler and E.A. Wolicki, "Surface Analysis of Gold and Platinum Disks by Activation Methods and by Prompt Radiation From Nuclear Reactions," in *Modern Trends in Activation Analysis* (J.R. DeVoe, ed.), NBS Special Publication 312, Vol. II, Government Printing Office, Washington, D.C., 1969, p. 791.

23. C. Engelmann, J. Gosset, M. Loeuillet, A. Marschal, P. Ossart, and M. Boissier, "Examples of Determination of Light Elements in Various High Purity Materials by Gamma Photon and Charged Particle Activation," in *Modern Trends in Activation Analysis* (J.R. DeVoe, ed.), NBS Special Publication 312, Vol. II, Government Printing Office, Washington, D.C., 1969, p. 819.

24. A.R. Knudson and K.L. Dunning, "Detection of Chlorine on Aluminum by Means of Nuclear Reactions," to be published in Analytical Chemistry (June 1972).

25. R.C. Koch, *Activation Analysis Handbook*, Academic Press, New York, 1960.

26. *Activation Analysis, A Bibliography* (G.J. Lutz, R.J. Boreni, R.S. Maddock, and W.W. Meinke, eds.), NBS Technical Note 467, Parts 1 and 2, Government Printing Office, Washington, D.C., May 1971.

27. C. Williamson, J. Borojot, and J. Picard, "Tables of Charged Particle Energy Losses," CEA-R3042, Commissariat a l'Energie Atomique, Paris, 1966.

28. D.M. Holm, J.A. Basmajian, and W.M. Sanders, "Observations of the Microscopic Distribution of Oxygen and Carbon in Metals by He^3 Activation," Los Alamos Scientific Laboratory Report LA-3515, 1966.

29. J.C. Ritter, M.N. Robinson, B.J. Faraday, and J.I. Hoover, "Room Temperature Oxidation of Silicon During and After Etching," J. Phys. Chem Solids **26**, 721 (1965).

30. C.A. Carosella and J. Comas, "Oxygen Sticking Coefficients on Clean (111) Silicon Surfaces," Surface Sci. **15**, 303 (1969).

31. J.A. Cookson and F.D. Pilling, "A 3 MeV Proton Beam of Less Than Four Microns Diameter," AERE-R-6300, Atomic Energy Research Establishment, Harwell, Berks, England, 1970.

32. T.B. Pierce, "The Examination of Surfaces By Scanning With Charged Particle Beams," Proc. Soc. Anal. Chem. **7**, 59 (1970).

33. S. Rubin, T.O. Passell, and L.E. Bailey, "Chemical Analysis of Surfaces by Nuclear Methods," Anal. Chem **29**, 736 (1957).

34. A.L. Turkevich, E.J. Franzgrote, and J.H. Patterson, "Chemical Analysis of the Moon at the Surveyor V Landing Site," Sci. **158**, 635 (1967).

35. O.U. Anders, "Use of Charged Particles From a 2 Megavolt Van de Graaff Accelerator for Elemental Surface Analysis," Anal. Chem. **38**, 1442 (1966).

36. M. Peisach and D.O. Poole, "The Use of Semiconductor Detectors for Surface Analysis by Elastic Scattering of Accelerated Charged Particles," in *Proceedings of the 1965 International Conference on Modern Trends in Activation Analysis* (J.P. Guinn, ed.), Texas A&M U., College Station, Texas, 1965, p. 206.

37. E. Bøgh and E. Uggerhøj, "Experimental Investigation of Orientation Dependence of Rutherford Scattering Yield in Single Crystals," Nuc. Inst. Methods **38**, 216 (1965).

38. D.P. Smith, "Scattering of Low-Energy Noble Gas Ions from Metal Surfaces," J. Appl. Phys. **38**, 340 (1967).

39. D.A. Thompson, H.D. Barber, and W.D. Mackintosh, "The Determination of Surface Contamination on Silicon by Large Angle Ion Scattering," Appl. Phys. Lett. **14**, 102 (1969).

40. O. Meyer, J. Gyulai, and J.W. Mayer, "Analysis of Amorphous Layers on Silicon by Backscattering and Channeling Effect Measurements," Surface Sci. **22**, 263 (1970).

41. I.V. Mitchell, M. Kamoshida, and J.W. Mayer, "Channeling-Effect Analysis of Thin Films on Silicon: Aluminum Oxide," J. Appl. Phys. **42**, 4378 (1971).

42. J. Gyulai, J.W. Mayer, I.V. Mitchell, and V. Rodriguez, "Outdiffusion Through Silicon Oxide and Silicon Nitride Layers on Gallium Arsenide," Appl. Phys. Lett. **17**, 332 (1970).

43. T.B. Pierce, P.F. Peck, and D.R.A. Cuff, "Examination of Contamination on the Surface of an Alumina Insulator by Elastic α-Particle Scattering," J. Inorg. Nucl. Chem. **33**, 1963 (1971).

44. S.T. Picraux and F.L. Vook, "Multilayer Thin-Film Analysis by Ion Backscattering," Appl. Phys. Lett. **18**, 191 (1971).

45. M. Croset, S. Rigo, and G. Amsel, "Investigation of the Composition of Sputtered Silicone Nitride Films by Nuclear Microanalysis," Appl. Phys. Lett. **19**, 33 (1971).

46. A. van Wijngaarden, B. Miremadi, and W.E. Baylis, "Energy Spectra of keV Backscattered Protons as a Probe for Surface-Region Studies," Can. J. Phys. **49**, 2440 (1971).

47. D.P. Smith, "Analysis of Surface Composition with Low-Energy Backscattered Ions," Surface Sci. **25**, 171 (1971).

48. A. Hiraki, M.A. Nicolet, and J.W. Mayer, "Low-Temperature Migration of Silicon in Thin Layers of Gold and Platinum," Appl. Phys. Lett. **18**, 178 (1971).

49. B.L. Cohen, C.L. Fink, and J.H. Degnan, "Nondestructive Analysis for Trace Amounts of Hydrogen," J. Appl. Phys. **43**, 19 (1972).

50. T.M. Buck and G.H. Wheatley, "Studies of Solid Surfaces with 100 keV $^4He^+$ and H^+ Ion Beams," Surface Sci. **33**, 35 (1972).

51. R.L. Meek and W.M. Gibson, "Determination of Lighter Impurities on Silicon by 90° Forward Ion Scattering Through Thin Targets," Nucl. Inst. Methods **98**, 375 (1972).

52. J.K. Hirvonen, W.H. Weisenberger, J.E. Westmoreland, and R.A. Meussner, "Backscattering Investigation of Low Temperature Migration of Chromium Through Gold Films," to be published in Applied Physics Letters.

53. J.U. Andersen, "Axial and Planar Dips in Reaction Yield for Energetic Ions in Crystal Lattice," Mat. Fys. Medd. Dan. Vid. Selsk. **36**, No. 7 (1967).

54. E. Bøgh, "Interaction of Radiation with Solids," *Proceedings of Cairo Solid State Conference, American University in Cairo*, 1966 (A. Bishay, ed.), Plenum Press Inc., New York, 1967.

55. J.A. Davies, J. Denhartog, L. Eriksson, and J.W. Mayer, "Ion Implantation of Silicon. I. Atom Location and Lattice Disorder by Means of 1.0-MeV Helium Ion Scattering," Can. J. Phys. **45**, 4053 (1967).

56. F.H. Eisen, B. Welch, J.E. Westmoreland, and J.W. Mayer, "Lattice Disorder Produced in Silicon by Boron Ion Implantation," *Proceedings of International Conference on Atomic Collision Phenomena in Solids*, Univ. of Sussex, Brighton, England, 1969 (North Holland Pub. Co., 111, 1970).

57. R.R. Hart, H.L. Dunlap, and O.J. Marsh, "Disorder Produced in SiC by Ion Bombardment," Radiat. Eff. 9, 261 (1971).

58. J.W. Mayer, L. Eriksson, S.T. Picraux, and J.A. Davies, "Ion Implantation of Silicon and Germanium at Room Temperature. Analysis by Means of 1.0-MeV Helium Ion Scattering," Can. J. Phys. 46, 663 (1968).

59. W.H. Weisenberger, S.T. Picraux, and F.L. Vook, "Low Temperature Channeling Measurements of Ion Implantation Lattice Disorder in GaAs," Radiat. Eff. 9, 121 (1971).

60. J.E. Westmoreland, J.W. Mayer, F.H. Eisen, and B. Welch, "Analysis of Disorder Distributions in Boron Implanted Silicon," in *Proceedings of the International Conference on Ion Implantation in Semiconductors*, Thousand Oaks, Calif. 1970, Radiat. Eff. 6, 161 (1970).

61. L. Eriksson, J.A. Davies, N.G.E. Johansson, and J.W. Mayer, "Implantation and Annealing Behavior of Group III and V Dopants in Silicon as Studied by the Channeling Technique," J. Appl. Phys. 40, 842 (1969).

62. F.H. Eisen, "New Aspects of Atom Location: Flux Peaking," in *Proceedings of the II International Conference on Ion Implantation in Semiconductors* (I. Ruge and J. Graul, eds.), Garmisch-Partenkirchen, Bavaria, Germany, Springer-Verlag, New York, 1971, p. 287.

63. R.B. Alexander, G. Dearnaley, D.V. Morgan, J.M. Poate, and D. Van Vliet, "Lattice Site Location Measurements and Their Interpretation," in *Proceedings of European Conference on Ion Implantation*, Sept. 7-9, 1970, Reading, England, published by Peter Peregrinus Ltd, Stevenage, Herts., England, 1970, p. 181.

64. Hj. Matzke, J.A. Davies, and N.G.E. Johansson, "A channeling Study of the Structure of U_4O_9," Can. J. Phys. 49, 2215 (1971).

65. J.A. Davies, "Channeling — A New Tool in Crystallography and Solid State Investigations," Physi. Can. 23, No. 3, 13 (1967).

66. W.M. Gibson, "Particle Channeling Experiments Using Small Accelerators," *Proceedings of the Conference on the Use of Small Accelerators For Teaching and Research*, Oak Ridge Associated Universities, Oak Ridge Tennessee, April 8-10, 1968 (J.L. Duggan, ed.).

67. J.A. Davies, "Rutherford Scattering and Channeling: A Useful Combination for Studying Crystal Surfaces," J. Vacuum Sci. Technol. 8, 487 (1971).

68. *European Conference on Ion Implantation*, Reading, England, Sept. 7-9, 1970, published by Peter Peregrinus Ltd, Stevenage, Herts., England, 1970.

69. F.H. Eisen and L.T. Chadderton, eds., *Ion Implantation*, Gordon Breach Science Publishers, Inc., New York, 1971.

70. I. Ruge and J. Graul, eds., *Proceedings of the II International Conference on Ion Implantation in Semiconductors*, Garmisch-Partenkirchen, Bavaria, Germany, Springer-Verlag, New York, 1971.

71. J.W. Mayer, L. Eriksson, and J.A. Davies, *Ion Implantation in Semiconductors*, Academic Press, New York (1970).

72. J. Gyulai, O. Meyer, J.W. Mayer, and V. Rodriguez, "Analysis of Silicon Nitride Layers on Silicon by Backscattering and Channeling Effect Measurements," Appl. Phys. Lett. **16**, 232 (1970).

73. I.V. Mitchell, M. Kamoshida, and J.W. Mayer, "Lineshape Extraction From MeV He^+ Backscattering Energy Spectra: Aluminum Oxide on Silicon," Phys. Lett. **35A**, 21 (1971).

74. A.G. Pieper and R.B. Theus, "Cyclotron Helium Implantation," in "Cooperative Radiation Effects Simulation Program," NRL Memorandum Report 2394, Naval Research Laboratory, Washington, D.C., Feb. 1972.

75. T.A. Cahill, "Use of Alpha-Particle Excited X-Ray Emission for Analysis of Smog Aerosols," Bull. Am. Phys. Soc. Series II, **17** (No. 4), 505 (1972).

76. R.F. Goff and D.P. Smith, "Surface Composition Analysis by Binary Scattering of Noble Gas Ions," J. Vacuum Sci. Technol. **7**, 72 (1970).

77. D.J. Ball, T.M. Buck, D. MacNair, and G.H. Wheatley, "Investigation of Low Energy Ion Scattering as a Surface Analytical Technique," Surface Sci. **30**, 69 (1972).

78. E. Everhart, G. Stone, and R.J. Carbone, "Classical Calculation of Differential Cross Section for Scattering from a Coulomb Potential with Exponential Screening," Phys. Rev. **99**, 1287 (1955).

79. W. Heiland and E. Taglauer, "Investigation of Surface Topography of Oxygen on Nickel Single Crystals by He Ion Backscattering," International Conference on Solid Surfaces, American Vacuum Society, Oct. 11-15, 1971, Boston, Mass. (1971).

80. L.S. Birks, R.E. Seebold, A.P. Batt, and J.S. Grosso, "Excitation of Characteristic X Rays by Protons, Electrons, and Primary X Rays," J. Appl. Phys. **35**, 2578 (1964).

81. D.M. Poole and J.L. Shaw, "Microanalysis with a Proton-Probe," Vth International Congress on X-Ray Optics and Microanalysis, Tübingen, 1968, G. Möllenstedt and K. H. Gaukler, eds., Springer-Verlag New York, 1969, p. 319.

82. T.B. Johansson, R. Akselsson, and S.A.E. Johansson, "X-Ray Analysis: Elemental Trace Analysis at the 10^{-12} g level," Nucl. Inst. Methods **84**, 141 (1970).

83. J.A. Cairns, C.L. Desborough, and D.F. Holloway, "A New End Window Variable Geometry X-Ray Proportional Counter," Nucl. Inst. Methods **88**, 239 (1970).

84. B.M. Gordon and H.W. Kraner, "Development of a System for Trace Element Analysis in the Environment by Charged Particle X-Ray Fluorescence," BNL-16182, Brookhaven National Laboratory, New York, 1971.

85. R.G. Flocchini, P.J. Feeney, R.J. Sommerville, and T.A. Cahill, "Sensitivity Versus Target Backings For Elemental Analysis by Alpha Exicted X-Ray Fluorescence," to be published in Nucl. Inst. Methods.

86. R.L. Watson, J.R. Sjurseth, and R.W. Howard, "An Investigation of the Analytical Capabilities of X-Ray Emission Induced by High Energy Alpha Particles," Nucl. Inst. Methods **93**, 69 (1971).

87. J.W. Verba, J.W. Sunier, B.T. Wright, I. Slaus, A.B. Holman, and J.G. Kulleck, "Limitations and Improvements of Trace Element Analysis With Proton Induced X-Rays," Paper presented at the International Conference on Chemical Analysis by Charged Particle Bombardment, L.A.R.N. Nemur, Belgium, Sept. 5-8, 1971.

88. P.K. Mueller, A. Alcocer, T.A. Cahill, R. Sommerville, and R. Flocchini, "Elemental Analysis by Alpha Excited X-Ray Fluorescence," paper presented at American Chemical Society, meeting, Los Angeles, Mar. 1972.

89. J.M. Khan, D.L. Potter, and R.D. Worley, "Proposed Method for Microgram Surface Density Measurements by Observation of Proton-Produced X-Rays," J. Appl. Phys. 37, 564 (1966).

90. J.A. Cairns and R.S. Nelson, "Selective X-Ray Generation By Heavy Ions, Part 1 — The Use of Energetic Heavy Ions to Generate Characteristic X-Rays from Elements in a Selective Manner," Radiat. Eff. 7, 163 (1971).

91. J.A. Cairns, D.F. Holloway, and R.S. Nelson, "Selective X-Ray Generation by Heavy Ions. Part 2, Measurement of the Concentration Distribution of Ion Implanted Antimony in silicon by the Use of Selective Heavy Ion X-Ray Excitation," Rad. Eff. 7, 167 (1971).

92. A.R. Knudson and P.E. Wilkniss private communication.

93. P.G. Burkhalter, A.R. Knudson, D.J. Nagel, and K.L. Dunning, "Chemical Effects in Ion-Excited Aluminum K X-Ray Spectra," in NRL Memorandum Report 2438, May 3, 1972, p. 13.

94. E.A. Wolicki and A.R. Knudson, "A Nuclear-Detection Method For Sulfur in Thin Films," Internat. J. Appl. Radiat. Isotop. 18, 429 (1967).

95. G. Amsel and D. Samuel, "Microanalysis of the Stable Isotopes of Oxygen by Means of Nuclear Reactions," Anal. Chem. 39, 1689 (1967).

96. G. Amsel, J.P. Nadai, E. D'Artemare, D. David, E. Girard, and J. Moulin, "Microanalysis by the Direct Observation of Nuclear Reactions Using a 2 MeV Van de Graaff," Nucl. Inst. Methods 92, 481 (1971).

97. J.N. Barrandon, L. Quaglia, J.L. Debrun, M. Cuypers, and G. Robaye, "Utilization of Low Energy Deuterons and Tritons for Measuring Carbon and Oxygen Present at the Surface of Metal Samples," J. Radio-Anal. Chem. 4, 115 (1970).

98. D.W. Palmer, "Oxygen Diffusion in Quartz Studied by Proton Bombardment," Nucl. Instr. Methods 38, 187 (1965).

99. E. Möller, L. Nilsson, and M. Starfelt, "Microanalysis of Light Elements by Means of (d,n) Reactions," Nucl. Inst. Methods 50, 270 (1967).

100. M. Peisach, "Analytical Use of Prompt Neutrons Produced by Pulses of Charged Particles," in *Proceedings of the 2nd Conference on Practical Aspects of Activation Analysis with Charged Particles*, (H.G. Ebert, ed.), European Communities, Brussels, Belgium, Mar. 1968, p. 650.

101. T. Joy and D.G. Barnes, "Some Practical Applications of the Observation of the ^{16}O-Direct Proton Capture Reaction With a Ge(Li) Detector," Nucl. Inst. Methods 95, 199 (1971).

102. K.L. Dunning, "Fortran Programs for (p,γ) Yield Calculations Based on Vavilov's Theory of Energy Loss Distributions," NRL Report 7230.

103. K.L. Dunning, "Aluminum in SiO_2; Depth Profiles by Means of a Nuclear Resonance Reaction," in NRL Memorandum Report 2438, Mar. 1972, p. 35.

104. R.O. Bondelid and C.A. Kennedy, "Precise Determination of Nuclear Reaction Energies and Measurements of Resonance Widths," Phys. Rev. **115**, 1601 (1959).

105. M.K. Bernett, J.W. Butler, E.A. Wolicki, and W.A. Zisman, "Relation between Residual Polishing Agent and Material Hardness Determined by a Narrow Nuclear-Reaction Resonance Technique," J. Appl. Phys. **42**, 5826 (1971).

106. E. Möller and N. Starfelt, "Microanalysis of Fluorine in Zircaloy by the Use of the $^{19}F(p,\alpha\gamma)^{16}O$ Reaction," Nucl. Inst. Methods **50**, 225 (1967).

107. J.F. Chemin, J. Roturier, B. Saboya, and G.Y. Petit, "Microanalysis of Si and S in GaSb by Direct Observation of Resonant Nuclear Reactions," Nucl. Inst. Methods **97**, 211 (1971).

108. J.L. Whitton, I.V. Mitchell, and K.B. Winterbon, "Depth Distribution of Implanted Oxygen in Gallium Phosphide Measured by Nuclear Reaction Techniques," Can. J. Phys. **49**, 1225 (1971).

Security Classification

DOCUMENT CONTROL DATA - R & D

(Security classification of title, body of abstract and indexing annotation must be entered when the overall report is classified)

1. ORIGINATING ACTIVITY (Corporate author)	2a. REPORT SECURITY CLASSIFICATION
Naval Research Laboratory Washington, D.C. 20390	Unclassified
	2b. GROUP

3. REPORT TITLE

NUCLEAR AND ION BEAM TECHNIQUES FOR SURFACE AND NEAR-SURFACE ANALYSIS

4. DESCRIPTIVE NOTES (Type of report and inclusive dates)

Survey report

5. AUTHOR(S) (First name, middle initial, last name)

Eligius A. Wolicki

6. REPORT DATE	7a. TOTAL NO. OF PAGES	7b. NO. OF REFS
December 13, 1972	53	108

8a. CONTRACT OR GRANT NO.	9a. ORIGINATOR'S REPORT NUMBER(S)
b. PROJECT NO.	NRL Report 7477
c.	9b. OTHER REPORT NO(S) (Any other numbers that may be assigned this report)
d.	

10. DISTRIBUTION STATEMENT

Approved for public release; distribution unlimited.

11. SUPPLEMENTARY NOTES	12. SPONSORING MILITARY ACTIVITY

13. ABSTRACT

A survey is made of recent developments in the applications of ion beam techniques to surface analyses. Ion beams are taken to be charged atomic species such as protons, deuterons, helium-3, alpha particles, and others and the energies of interest, usually, but not always, are in the range from one million electron volts (MeV) upward. The discussion covers not only those techniques which are presently ready for application but also those which are still being investigated and developed in the laboratory. The objective of the discussion is to give the reader an overview of the present state of the art and, hopefully, sufficient information so that he can assess, for his own problems, whether a given technique may have advantages over more standard techniques.

Techniques are categorized according to whether they are based on charged particle activation analysis or on prompt radiation analysis. The discussion emphasizes prompt radiation analysis since this area is in general newer and less well known than is charged particle activation analysis. Subcategories discussed under prompt radiation analysis include: (a) high-energy backscattering, (b) channeling, (c) high-energy forward scattering, (d) low-energy backscattering, (e) heavy-ion-induced x rays, (f) nuclear reactions, and (g) nuclear resonance reactions. Numerous examples of actual analyses are discussed for each category. A comprehensive list of references, totaling 108 in number, is given.

14. KEY WORDS	LINK A		LINK B		LINK C	
	ROLE	WT	ROLE	WT	ROLE	WT
Activation analysis						
Analysis by nuclear reactions						
Backscattering						
Channeling						
Charged particle activation analysis						
Charged particle beams						
Crystal imperfections						
Elastic scattering						
Elemental analysis						
Gas analysis						
Heavy ion induced x-rays						
Impurity concentration profiles						
Ion beam applications						
Ion beam irradiations						
Ion beam techniques						
Ion implantation						
Isotopic analysis						
Materials analysis						
Microbeam analysis						
Nuclear applications						
Nuclear reactions						
Nuclear resonance reactions						
Nuclear techniques						
Prompt radiation analysis						
Qualitative analysis						
Quantitative analysis						
Rearrangement collisions						
Surface analysis						
Thin film analysis						
Trace element analysis						
Trace element standards						
X-rays						